Fetal MRI of Normal Brain Development

Denise Pugash, Ursula Nemec, Peter C. Brugger, and Daniela Prayer

Contents

Abstract

› The fetal brain is substantially different from the neonatal brain in terms of its structure and connectivity. Fetal MRI, beginning at 16–18 GW (gestational weeks), can be used to study fetal brain development and maturation in vivo. T2-weighted (T2W), T1-weighted (T1W), and diffusion-weighted (DW) imaging sequences can be used primarily to demonstrate morphology, parenchymal lamination, sulcation and gyration, the width of the subarachnoid spaces, and the size and shape of the midline structures. It is essential to understand MR signal changes associated with maturation, including the appearance and disappearance of transient structures,

D. Pugash (✉)
Departments of Radiology and Obstetrics and Gynecology, Division of Maternal-Fetal Medicine,
British Columbia Women's Hospital and
University of British Columbia, 1T48 - 4500 Oak Street
Vancouver, Canada V6H 3N1
e-mail: dpugash@cw.bc.ca

U. Nemec and D. Prayer
University Clinics of Radiodiagnostics and Medical University of Vienna, Waehringerguertel 18-20, 1090, Wien, Austria
e-mail: daniela.prayer@meduniwien.ac.at

P.C. Brugger
Integrative Morphology Group, Centre of Anatomy and Cell Biology, Medical University of Vienna, Waehringerstrasse 13, 1090, Vienna, Austria
e-mail: peter.brugger@meduniwien.ac.at

D. Prayer (ed.), *Fetal MRI*, Medical Radiology,
DOI: 10.1007/174_2010_116, © Springer-Verlag Berlin Heidelberg 2011

the underlying histological development of the fetal brain as well as the timing of development of landmarks in maturation in order to interpret normal and abnormal findings. It is the basis for understanding how neurogenetic development can be disrupted during vulnerable periods by different pathological processes, and how genetically controlled events in development correlate with functional development. The maturational stages of the fetal cerebral cortex, white matter, temporal lobe, and cerebellum, including structures that appear transiently in the developing brain as shown by various MR sequences, will be reviewed in this chapter.

1 Introduction

Ultrasound remains the primary imaging method of choice in the first and early second trimesters and has been used to demonstrate landmarks in the development of the brain, and in particular developmental timing of sulcation of the cortical mantle (Toi et al. 2004). Newer generation technology is beginning to allow visualization of individual zones of cortical development (Fig. 1). However, the ability to visualize the entire brain is inherently limited due to the physical impedance of the cranial vault. MRI can, in contrast, provide information both about gross anatomical structures as well as histological microstructure.

Histological changes in tissue composition result in decreased water content and increased cell density (the latter mainly in the gray matter), which are reflected in shortening of T1 and T2 relaxation times, and correspondingly increased T1-weighted (T1W) signal intensity and decreased T2-weighted (T2W) signal intensity. Secondly, differences in microanatomical structures can be demonstrated by diffusion-weighted (DW) anisotropy, as well as premyelination of axons which affect the appearance of structures on DW sequences. Sequences used must provide optimal contrast at the respective gestational ages, and must reflect tissue properties such as cell density and impending myelination. In addition, proton spectroscopy can provide metabolic information, and assessment of fetal movement can be correlated with functional development of neural structures.

Imaging of the fetal brain has been done from the beginning of in vivo MRI (Daffos et al. 1988), relying upon the T2-weighted contrast between CSF spaces and brain which allowed accurate assessment of the development of the brain surface. This permitted the assessment of timing of normal sulcation and gyration (Garel et al. 2001).

Subsequently, in vitro studies of fetal brain development recognized that the fetal brain parenchyma before about 28 gestational weeks (GW) had a different appearance of cortical layering than that of older

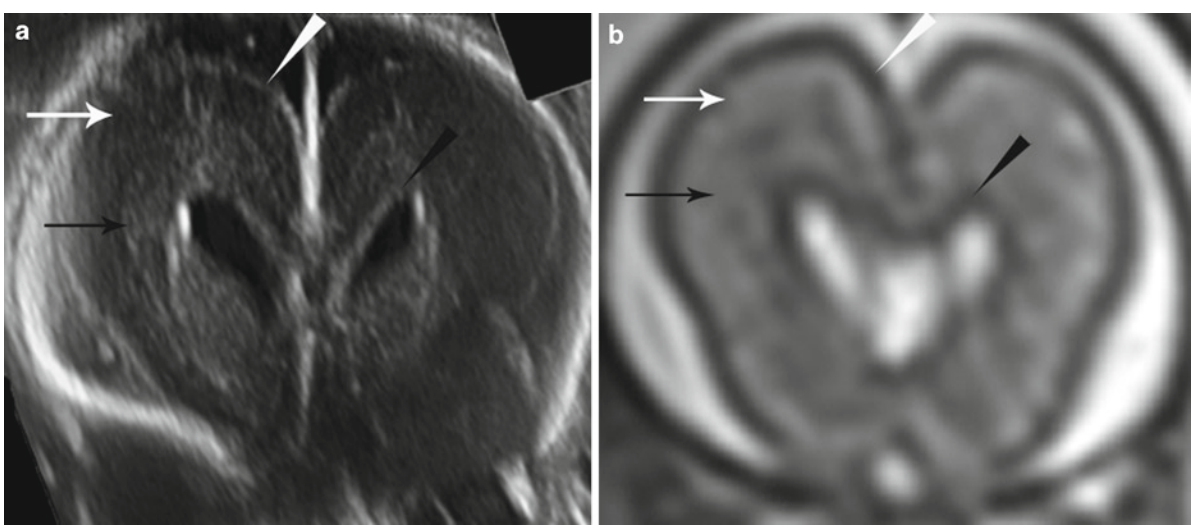

Fig. 1 Coronal view through the frontal horns using ultrasound at 19+3 GW (**a**) and T2-weighted MRI at 21 GW (**b**). High-resolution ultrasound technology allows visualization of individual zones of cortical development. However, the ability to visualize the entire brain is limited due to ossification of the cranial vault. Visible layers include the ventricular zone (*black arrowheads*), the intermediate zone (*black arrows*), the subplate (*white arrows*), and the cortical plate (*white arrowheads*)

fetuses (Kostovic et al. 2002). The morphological characterization of the different layers of the fetal brain parenchyma before 28 GW requires high-resolution T2-weighted contrast and/or diffusion-weighted information. T1-weighted contrast was shown to visualize regions of higher cell density, compared with surrounding structures (Brugger et al. 2006). Based on anisotropy that is present already in premyelinating white matter tracts (Wimberger et al. 1995), diffusion-tensor imaging and fibertracking can be performed (Kasprian et al. 2008). In addition, patterns of normal fetal movement and behavior have been defined, and can be documented using dynamic MR techniques.

2 Supratentorial Cortical Development

The primitive cerebral hemispheres are first seen at about 5 GW (3 GW after conception) as bilateral vesicles that protrude from the sides of the telencephalon in the area of the foramina of Monro (Muller and O'Rahilly 1988). The forebrain consists of the dorsal telencephalon or pallium which develops into the cerebral cortex and hippocampus, and the ventral telencephalon or subpallium which gives rise to the striatum and globus pallidus. The diencephalon gives rise to the thalamus and hypothalamus. In the initial stages, the wall of the cerebral vesicles is composed of a single layer of neuroepithelial cells (Marin-Padilla 1990). The cerebral vesicles grow and expand as neuroepithelial cells, located in the germinal ventricular zone, divide to form future cortical neurons beginning at 5 GW (Fishell et al. 1993; Levitt 2003). Layers of cells develop in the vesicles as they expand, forming the germinal matrices which are the origin of cells that will form the cerebral cortices. Initially, the germinal matrices are composed of a single zone, the ventricular zone. These cells are direct descendents of the neural plate, and differentiate into glial cells and neuroblasts (Brazel et al. 2003). The cortical plate begins to appear after the seventh gestational (fifth postconception) week, in the lateral aspect of the hemispheric wall (Bystron et al. 2006). At this stage, the forebrain wall contains two layers. The deeper layer consists of neuroepithelial cells and is termed the ventricular zone or germinal matrix. The more superficial layer is the preplate, which gives rise to the future cortex.

The vesicular walls are thin and are joined by the lamina terminalis in the midline. Cortical predecessor cells are thought to originate from the basal telencephalon, and migrate tangentially to the pia, arriving before cells from the ventricular zone begin radial migration to the preplate (Bystron et al. 2006). The cortical predecessor cells join neurons formed in the ventricular zone which migrate radially into the preplate, as well as Cajal–Retzius cells and neurons that have arrived by means of tangential migration (Bystron et al. 2008). The ventricular zone subsequently generates the first postmitotic or "pioneer" neurons that migrate radially into the preplate, dividing the preplate into two zones, the superficial marginal zone and the deeper subplate zone (Super and Uylings 2001). The outermost portion of the cortical plate is the marginal zone, and will become the future layer 1 of the mature cerebral cortex (Marin-Padilla 1990). Layer 1 also results from the first postmitotic cells from the ventricular zone (Samuelsen et al. 2003). It influences the laminar organization of the future cerebral cortex (ten Donkelaar 2000). This coincides with the end of the embryonic period and the beginning of the fetal period.

The germinal ventricular zone is the source of cells during embryonic and early fetal life. However, the subventricular zone, which is formed by the ventricular zone, increasingly becomes the source of neurons and glial cells when the ventricular zone begins to disappear in the third trimester (Brazel et al. 2003).

The ventricular zone generates waves of postmitotic neurons which migrate along radial glial cells, and form individual layers of neocortex. The ventricular zone produces deep-layer neurons of the future six-layer cortex, and the subventricular zone generates more superficially located neurons (Zecevic 1993). Layer 6 forms between the subplate and Cajal–Retzius cells. Layer 5 then forms between layer 6 and the marginal zone, resulting in formation of the cortex in an inside-out fashion (Marin-Padilla 1990).

Subsequently, the subventricular germinal zone develops laterally, separate from the ventricular zone, and is located between the ventricular zone and the intermediate zone. It also contains GABAergic interneurons originating in the lateral ganglionic eminence (in the third ventricular walls). These migrate tangentially to the walls of the lateral ventricles before

radial migration to the developing neocortex (Letinic et al. 2002; Marin and Rubenstein 2003). Migration to the developing cortex is complete for the most part by 26 GW (Marin-Padilla 1990). It is therefore evident that neuronal migration is occurring at a gestational age when fetal imaging is performed for clinical purposes.

There are four distinct areas within the ventricular/subventricular zone which include the medial, lateral, and caudal ganglionic eminences; and the neocortical subventricular zone. The ganglionic eminences are focal areas of thickening in the ventricular/subventricular zone which protrude into and shape the lateral ventricles (Brazel et al. 2003). The ganglionic eminences give rise to neurons which form the transient gangliothalamic body, parts of the amygdala, the basal nucleus of Meynert, the basal ganglia, and the thalamus (Letinic and Kostovic 1997; Ulfig 2002).

After 17 GW, the brain contains seven histological layers that are visible on in vitro MR images (Kostovic et al. 2002). These layers mature and evolve in thickness and number until 36 GW. At 18 GW, the ventricles appear prominent relative to the thickness of the cortex (Farrell et al. 1994). As gestation progresses, the thickness of the cortical mantle increases relative to the ventricle while the ventricular size remains unchanged (Prayer et al. 2006). As the basal ganglia enlarge, the ventricles assume their typical configuration. There is, therefore/subsequently, a relative decrease in size of the ventricles between 18 and 24 GW. Sulcation and gyration subsequently contribute to growth and increased thickness of the cortical mantle (Prayer et al. 2006) (Fig. 2).

Before 20 GW, a cortical plate forms within the preplate and gives rise to cortical layers 2–4 (Marin-Padilla 1998). Neurons migrate in radial as well as tangential fashion, with an exponential increase in numbers of cells (Corbin et al. 2001; Samuelsen et al. 2003; Fogliarini et al. 2005). The subplate zone, also known as layer 7 of the developing cortex, is visible beneath the cortical plate, and is a transient structure that is widest at 22 GW and cannot be delineated on fetal MR after 30 GW (Kostovic et al. 2002). It is formed when the preplate is divided by radial migration of streams of neurons from the ventricular zone. Neurons in the subplate are derived from the deepest layer of the preplate and are among the oldest population in the forebrain. The subplate contains a heterogeneous population of neurons with abundant extracellular matrix containing neurotransmitters and transient synapses (Bystron et al. 2008). Within the subplate layer, neurons are able to form temporary circuits between

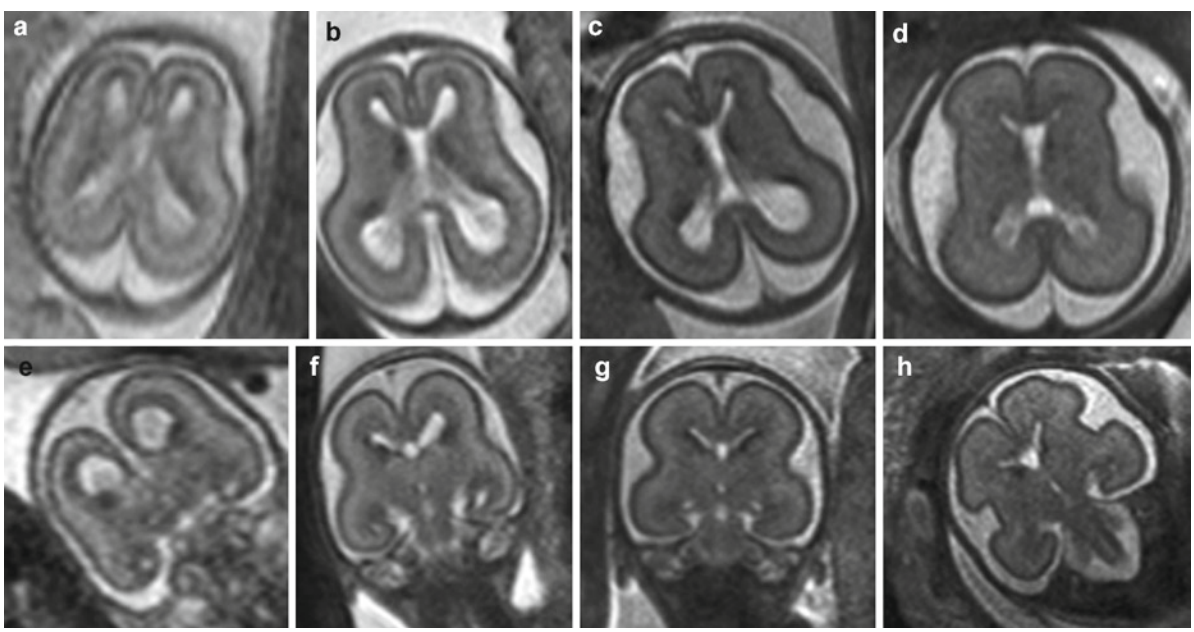

Fig. 2 Axial (*upper line*) and coronal (*lower line*) T2-weighted sequences of fetuses at 18+1 (**a**, **e**), 20+4 (**b**, **f**), 22+1 (**c, g**), and 24+0 (**d**, **h**) GW. Note the width of the ventricles and the thin brain parenchyma in the 18 GW fetus (**a, e**). Later, the thickness of the cortical mantle increases whereas the size of the ventricles decreases (**b–d, f–h**)

thalamus and cortex (Arber 2004). Cells are derived from the ventricular zone, the marginal zone, and the cortical plate (Kostovic et al. 1995).

Numerous functions have been attributed to the subplate zone, including that of an accumulation and waiting area for axons predetermined to synapse in the developing cortex, while their target cells migrate to the cortical plate, after which the axonal connections are established. This is important in the development of thalamocortical and other cortical afferent connections (Sur and Rubenstein 2005). The fetal white matter (external capsule fibers of the intermediate zone) forms the inferior border of the subplate (Kostovic et al. 2002). Subplate thickness varies in different locations of the brain. As axons move from the subplate to synapse in the cortex, the subplate progressively disappears after 34–36 GW (Kostovic and Jovanov-Milosevic 2008). The extracellular content of the subplate also decreases (Rados et al. 2006). Some cells persist as interstitial neurons in the subcortical white matter (Kostovic and Jovanov-Milosevic 2008).

In beginning of the preterm phase (26–33 GW), the subplate is very thick and can be easily distinguished from the cortical plate. After 34–36 GW, the subplate becomes thin and less well delineated from the cortical plate (Kostovic and Vasung 2009). The function of the subplate at this stage is related to the development of thalamocortical synaptic connections that form the first sensory circuitry which may be involved, for instance, in early pain processing (Lowery et al. 2007). Synaptogenesis increases with the development of the subplate (Kostovic et al. 1995). Due to the formation of specific axon-target interactions, neurons are "locked into position" once migration is complete (Samuelsen et al. 2003).

2.1 MRI Findings of Supratentorial Cortical Development

At 16 GW, in vitro, three layers can be differentiated in the cortical mantle by MRI, with the innermost and outermost layer appearing bright on T1-weighted and diffusion-weighted, and dark on T2W images. The intermediate layer shows relatively low signal on T1W images and high signal on T2W images compared to the inner and outer layers, corresponding to the intermediate zone which contains sparse neuroglial cells (Brisse et al. 1997). These layers, representing the ventricular/periventricular/subventricular zone, subplate and cortical plate (Kostovic et al. 2002), are difficult to delineate in vivo before GW 17–18. The intermediate zone, seen as a band between the ventricular/periventricular/subventricular zone, is usually detectable with intermediate signals of the respective sequence at the level of the frontal horns. After 17–18 GW, the cerebral mantle appears multilayered on in vitro as well as in vivo MR images until about 28–30 GW (Girard and Raybaud 1992; Chong et al. 1996; Brisse et al. 1997; Kostovic et al. 2002; Garel et al. 2003, 2004; Glenn and Barkovich 2006; Prayer et al. 2006) (Fig. 3). These layers are described as follows:

1. Ventricular zone – On T2W images, the germinal zone is hypointense, whereas, on T1W images it is hyperintense due to the high density of cell nuclei (Kinoshita et al. 2001; Maas et al. 2004) (Fig. 3a–d). It is of high signal intensity on DW images and is associated with a low ADC and medium-graded fractional anisotropy on scans of preterm neonates (Maas et al. 2004). The band of high signal intensity on DW source images, correlating with a dark band on ADC maps, corresponds with the intermediate, subventricular, periventricular, and germinal zone (Maas et al. 2004). (Fig. 3e). The hyperintensity may be due to high cell density as well as microvascularity which is more prevalent in the germinal zone than any other part of the developing brain (Ballabh et al. 2004), as well as the lack of radial organization (Maas et al. 2004).
2. Subventricular zone – The subventricular zone is thick in the frontal area and can be differentiated from other layers (Zecevic et al. 1999) (Fig. 3b). The subventricular zone contains germinal matrix that increases cell production as the ventricular zone disappears.
3. Intermediate zone – The intermediate zone is of slightly lower T1 signal intensity relative to the subplate layer (Widjaja et al. 2010a), between the subplate and the subventricular zone. (Fogliarini et al. 2005) (Fig. 3d). Together with the subventricular zone, it appears as a band of somewhat hypointense T2 signal subplate layer relative to ventricular zone and cortex (Fig. 3a–c). The intermediate zone contains axonal strata (Kostovic and Judas 2002) containing migratory neurons and glial cells, which results in moderate signal intensity on both T1 and T2W images (Kostovic and Vasung 2009) (Fig. 3a, d).

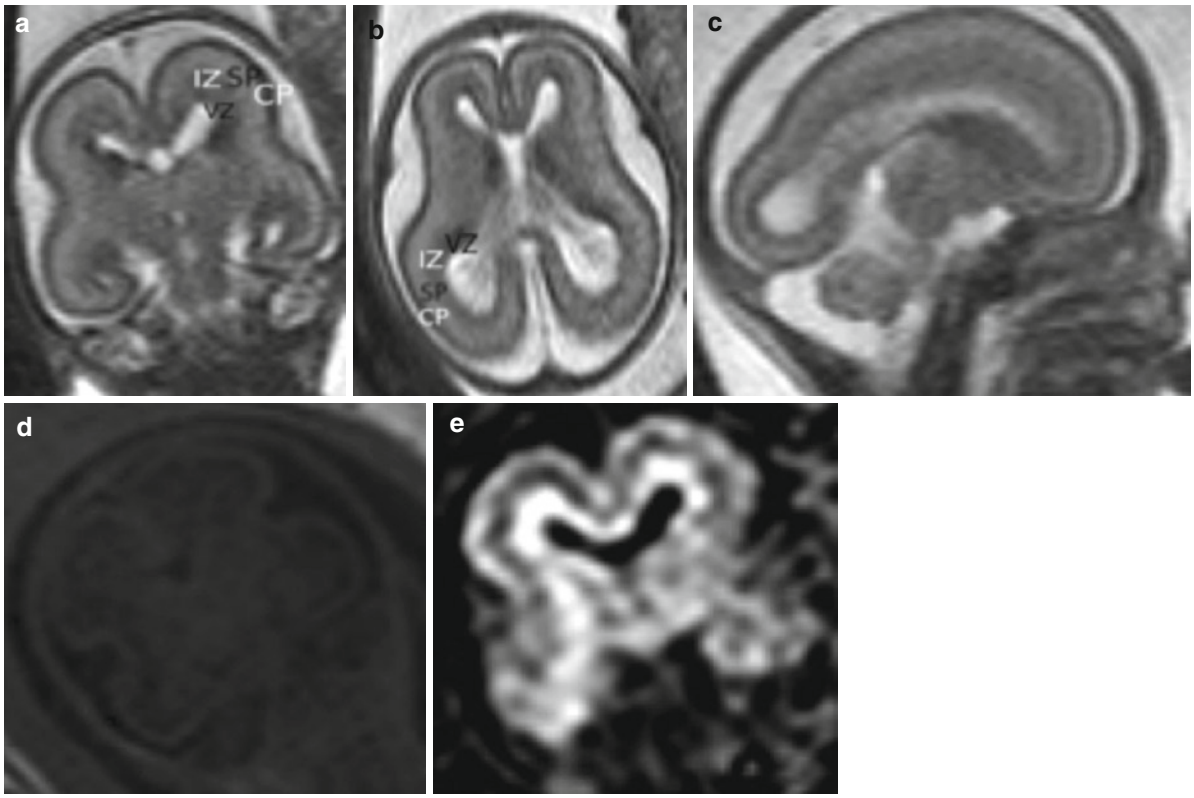

Fig. 3 T2-weighted sequences of a 20+4 GW fetus ((**a**) coronal T2 (**b**) axial T2 (**c**) sagittal). Note the layered organization of the fetal brain. The cortical plate (*CP*) appears hypointense, the subplate (*SP*) is hyperintense. The slim hypointense intermediate zone (IZ) and the hypointense ventricular zone (*VZ*) follow. On T1-weighted images the cortical plate is hypointense ((**d**) coronal). On diffusion-weighted sequences ((**e**) coronal), the cortical plate appears anisotropic

4. Subplate – The subplate zone has high water content due to extracellular matrix (Kostovic et al. 2002). On T2W images, the subplate is hyperintense (Fig. 3a–c), and it is hypointense to the cortical plate on T1W images (Fig. 3d). The subplate is hypointense on DW source images, and does not show evidence of anisotropy (Fig. 3e). These typical findings may be due to the amount of extracellular matrix and by the presence of axons that are not uniformly aligned and do not allow anisotropic behavior. The subplate band is thinner on DW images than on T2W sequences. (Fig. 3a, e). This reflects the inhomogeneity of the subplate due to fiber bundles which curve as they emerge from the thalamus (Prayer et al. 2006).
5. Cortical plate – The developing cortex appears hypointense on T2W images and hyperintense on T1W sequences relative to the subplate (Fig. 3a–d). On DW sequences, the cortical plate shows anisotropic behavior since it contains radially oriented migrating neurons (McKinstry et al. 2002; Maas et al. 2004) (Fig. 3e).

The layered appearance of the brain persists until around 28 GW, when decreasing T2W hyperintensity and increasing hypointensity of the subplate zone becomes isointense to the intermediate zone, and thus cannot be differentiated (Fig. 4). Alteration in lamination between 20 and 25 GW is due to gradual reduction in high T1 signal intensity and increase in low T2 signal intensity from about 22 weeks, found in both postmortem brains as well as antenatal T2W images (Widjaja et al. 2010b). This occurs prior to the histological disappearance of the subplate zone. The change in signal properties is most likely due to decreased water content of the extracellular matrix due to increased cellularity as axons "wait" in the upper subplate zone before moving to the more superficial developing cortex, as well as increased thickness of deep projecting fibers (Rados et al. 2006). The subplate

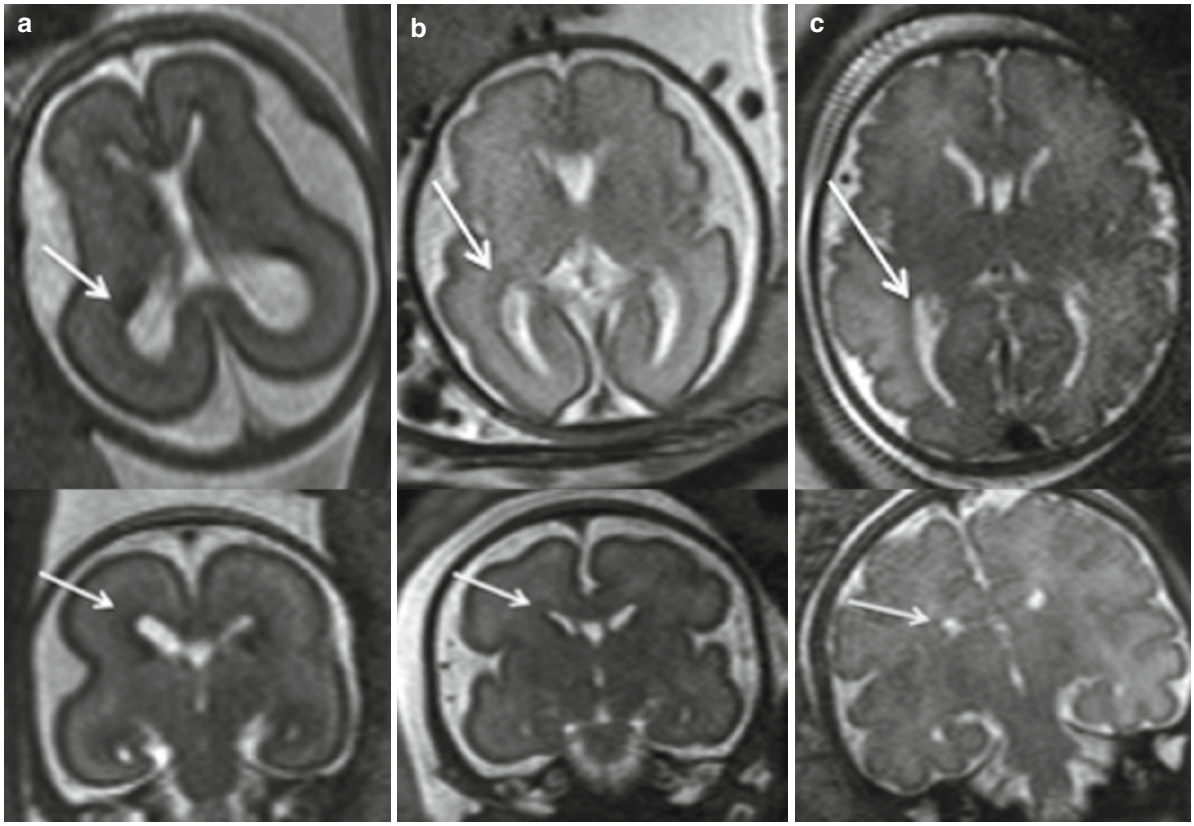

Fig. 4 T2-weighted fetal images at 20+4 (**a**), 28+1 (**b**), and 36+6 (**c**) GW. Upper images are in the axial plane, lower images are coronal. The subplate becomes isointense to the intermediate zone with increasing gestational age and cannot be differentiated. *Arrows* indicate areas where the subplate persists longest

persists longest in the frontal and temporal lobes on histological studies, and this has been observed in vivo as well (Rutherford et al. 2008) (Fig. 4).

Changes in cortical mantle development are also reflected in DW images. Mean diffusivity decreases in white matter with increasing gestational age and cortical thickening, due to synaptogenesis (Prayer and Prayer 2003; Bui et al. 2006; Manganaro et al. 2007; Schneider et al. 2007, 2009). Anisotropy disappears first in the central areas, then occipital cortex, and persists in the frontal and temporal areas until 35 GW (McKinstry et al. 2002; Maas et al. 2004; Fogliarini et al. 2005) (Fig. 5). DW imaging has also shown evidence of faster maturation of the right-sided frontal cortex relative to the left side, based on different values of fractional anisotropy (Gupta et al. 2005).

The appearances of the developing brain as well as biometric norms have been evaluated in a number of studies (Garel et al. 2003; Parazzini et al. 2008; Chung et al. 2009; Tilea et al. 2009).

3 Normal Sulcation and Gyration

Proposed hypotheses to explain the mechanisms of sulcal formation include sulcation resulting from cortical growth (Toro and Burnod 2005), variable growth between inner and outer cortical layers, and mechanical pulling by tethered axonal and glial fibers (Van Essen 1997; Hilgetag and Barbas 2005). Gyral development is most rapid in areas of sensory and visual pathways, which are the first areas to myelinate (Barkovich et al. 1988). Since sulcation is more predictable and uniform in areas of basic function such as motor and visual cortex, and more variable in areas of higher cortical function, sulcal formation may be related to variability and complexity of cortical connections (Fischl et al. 2008). Asymmetry in sulcation between right and left hemispheres, for example, with the left Sylvian fissure being longer than the right, has been noted both postmortem in fetuses (Chi et al. 1977) as well as on fetal MRI (Prayer et al. 2006; Chung

et al. 2009; Kasprian et al. 2010). Gyral development is later in the frontobasal, frontopolar, and anterior temporal areas, which are also slower to myelinate and to become metabolically mature (Penrice et al. 1996).

Cortical gyration occurs relatively late in fetal life. In the first half of gestation, the brain has a smooth, lissencephalic surface (Fig. 6a, b). In the second half of pregnancy, the brain surface gradually becomes more complex with a specific pattern of rapid development of gyri and sulci in the third trimester. Sulcation has been divided into 3 groups based on time of appearance and individual variability: primary, secondary, and tertiary. Primary sulci develop in parallel with the growth of the cerebral hemispheres, and are thought to reflect normal neurogenesis and orderly neuronal migration. The development of secondary sulci occurs at the same time as synaptogenesis begins to develop in the cortical plate.

Developmental appearance and localization of primary sulci are characterized by major cellular proliferative events. The appearance of the primary sulci coincides with thalamocortical axons reaching their destinations in the cortical plate (Kostovic and Judas 2002). As the cortex matures, the fissures and sulci become deeper, and the gyri expand. After 24–26 GW, gyration accelerates, and long corticocortical connections become established, characterized by the appearance of secondary sulci. (Kostovic 1990; Kostovic and Judas 2002, 2006). Tertiary sulcation begins after 28 GW (Garel et al. 2004; Fogliarini et al. 2005). At term and after birth, short corticocortical fibers reach their targets and the brain biomes highly convoluted with the development of highly variable tertiary sulci (Kostovic 1990; Kostovic and Judas 2002, 2006).

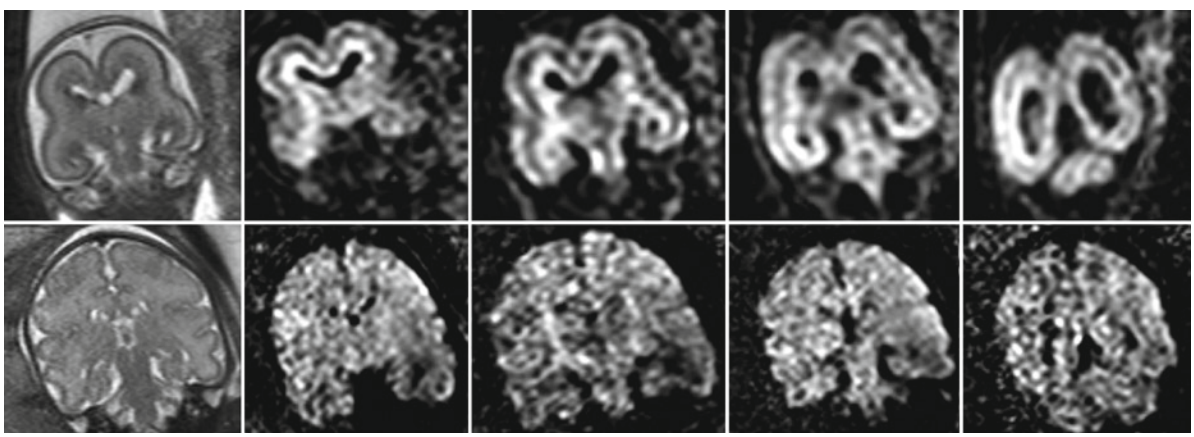

Fig. 5 Coronal diffusion-weighted sequences of fetuses at 20+4 GW (*upper*) and at 36+6 GW (*lower*). On the left are similar T2-weighted sequences. Note the changes in cortical mantle, particularly the disappearance of anisotropy and of the different layers (*lower line*)

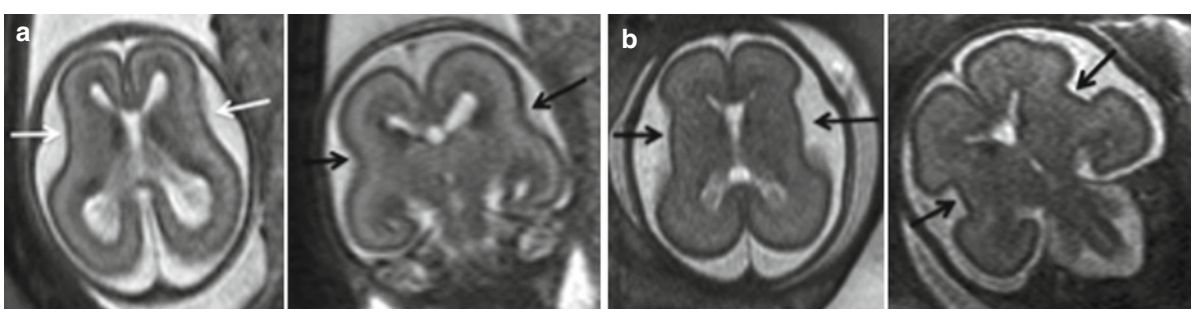

Fig. 6 T2-weighted sequences of fetuses at 20+4 GW ((**a**) left image, axial; right image, coronal) and at 24+0 GW ((**b**) left image, axial; right, coronal). Before 24 GW, the brain is agyric, and only the widely open obtusely angled Sylvian fissures can be recognized (*arrows*)

Since the appearance and development of sulci in the fetal brain follows a predictable pattern, the degree of sulcation may be used as an indicator of gestational age-related cortical development, both at autopsy and in vivo with fetal MRI (Chi et al. 1977; Dorovini-Zis and Dolman 1977; Garel et al. 2001, 2003). However, there is no clear consensus as to whether external landmarks of sulcation are reliable for gestational age estimation (Kostovic and Vasung 2009). This may in part be ascribed to inaccuracies in dating the autopsy specimens themselves in studies in which comparisons are based, different techniques for examining the fetal brains, and limited numbers of specimens in the studies. In particular, some postmortem studies of brain maturation rely on last menstrual period as the sole criterion of gestational age. One study (Chi et al. 1977) included specimens with a gestational age of 44 GW, which in itself probably reflects substantial errors in dating pregnancies. Moreover, delayed sulcation of 2–3 GW in twins before 32 GW as compared to singleton gestations, as well as asymmetry of maturation of the hemispheres, with the sulci appearing 1–2 GW earlier on the left side than the right side, introduces further error in establishing gestational age. Sulcation on fetal MRI appears to temporally lag by an average of two GW when compared with autopsy specimens (Levine and Barnes 1999; Garel et al. 2001, 2003). Comparisons may also be discrepant due to limitations in resolution of fetal MRI due to minimum voxel size and partial volume averaging (Chung et al. 2009). Also, there is a 2-week difference in when a sulcus can be detected initially, and when it can be recognized in 75% of fetuses (Garel et al. 2001). Cortical maturation has been assessed using sonography in both preterm neonates (van der Knaap et al. 1996; Dubois et al. 2008)and in the antenatal population (Toi et al. 2004).

3.1 MRI Appearance of Sulcation

Cortical gyration begins to be visible on MR images at 18 GW, starting with the shallow bitemporal indentations of the future Sylvian fissures. Before 24 GW, the brain is agyric apart from the widely open, obtusely angled Sylvian fissures (Fig. 6). The brain is very small and the cortex is extremely thin, therefore thin imaging sections are required (3 mm or less). By 23 GW, Sylvian fissures are more angular, and the parietooccipital sulcus and the callosal sulcus are detected in 75% of fetuses (Garel et al. 2001, 2003, 2004) (Fig. 7). The calcarine sulcus is visible by 24–25 GW in 75% of fetuses, and the central sulcus by 26 GW in 75%. The precentral and postcentral gyri can be identified in 75% by 27 and 28 GW, respectively. All primary and some secondary sulci are visible on fetal MRI by 34 GW (Garel et al. 2001, 2003; Garel 2004; Garel et al. 2004). Since very little sulcation is present prior to 24 GW, a suspected sulcal abnormality should be assessed later in gestation, ideally after 28 GW, when most of the primary sulci should be visible.

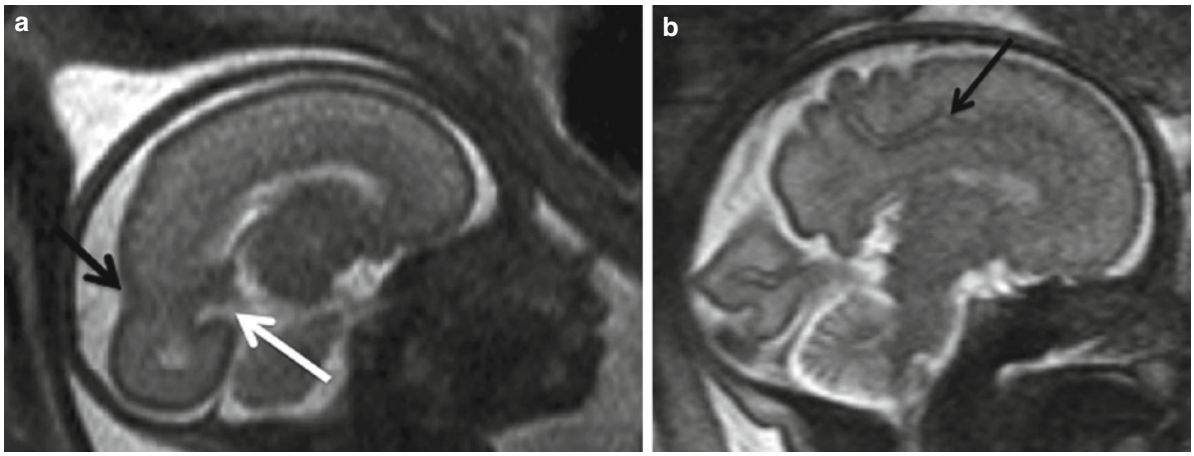

Fig. 7 Sagittal T2-weighted sequences of a fetus at 24+0 GW (**a**) and 32+0 GW (**b**). On image (**a**) the parieto-occipital sulcus (*black arrow*) and the calcarine sulcus (*white arrow*) are visible. Note the cingulate gyrus on image (**b**)

4 Development of the Temporal Lobe

A primordial hippocampus and hippocampal fissure begin to develop on the medial aspect of the telencephalon from the dorsal part of the lamina reuniens of His and can be identified histologically in the ninth GW (Rakic and Yakovlev 1968). Hippocampal cells originate from the ventricular zone of the dorsal forebrain and migrate radially to establish the temporal lobe. In addition, cells arise from the ganglionic eminence of the ventral forebrain and migrate tangentially to the cortical plate of the developing hippocampus, which is formed in an "inside-out manner" (Marin and Rubenstein 2003).

At 17–24 GW, the hippocampal formation displays a characteristic convoluted appearance and progressive narrowing of the cortical plate (Rados et al. 2006). In vitro, the hippocampal formation is the only part of the cerebral cortex in which the marginal zone is thick enough to be visualized by MRI. The increased thickness is due to transiently enlarged extracellular spaces, similar to that in the transient subplate zone elsewhere (Kostovic 1990). It forms a thin stripe of low signal on T1W images superficial to the hippocampal cortical plate which has high signal intensity (Rados et al. 2006). At 13–14 GW, on in vitro MR, the unfolded hippocampus surrounds the widely open hippocampal sulcus (hippocampal fissure) on the medial surface of the temporal lobe (Kier et al. 1997). At 15–16 GW, the dentate gyrus and cornu ammonis begin to fold inward. The hippocampal sulcus remains open, and the parahippocampal gyrus is larger and more medial in position. By 18–20 GW, the hippocampus begins to assume a more adult configuration, with the dentate gyrus and cornu ammonis folded within the temporal lobe (Fig. 8). The hippocampal sulcus is narrow and separates the closely apposed hippocampus and subiculum (Kier et al. 1997).

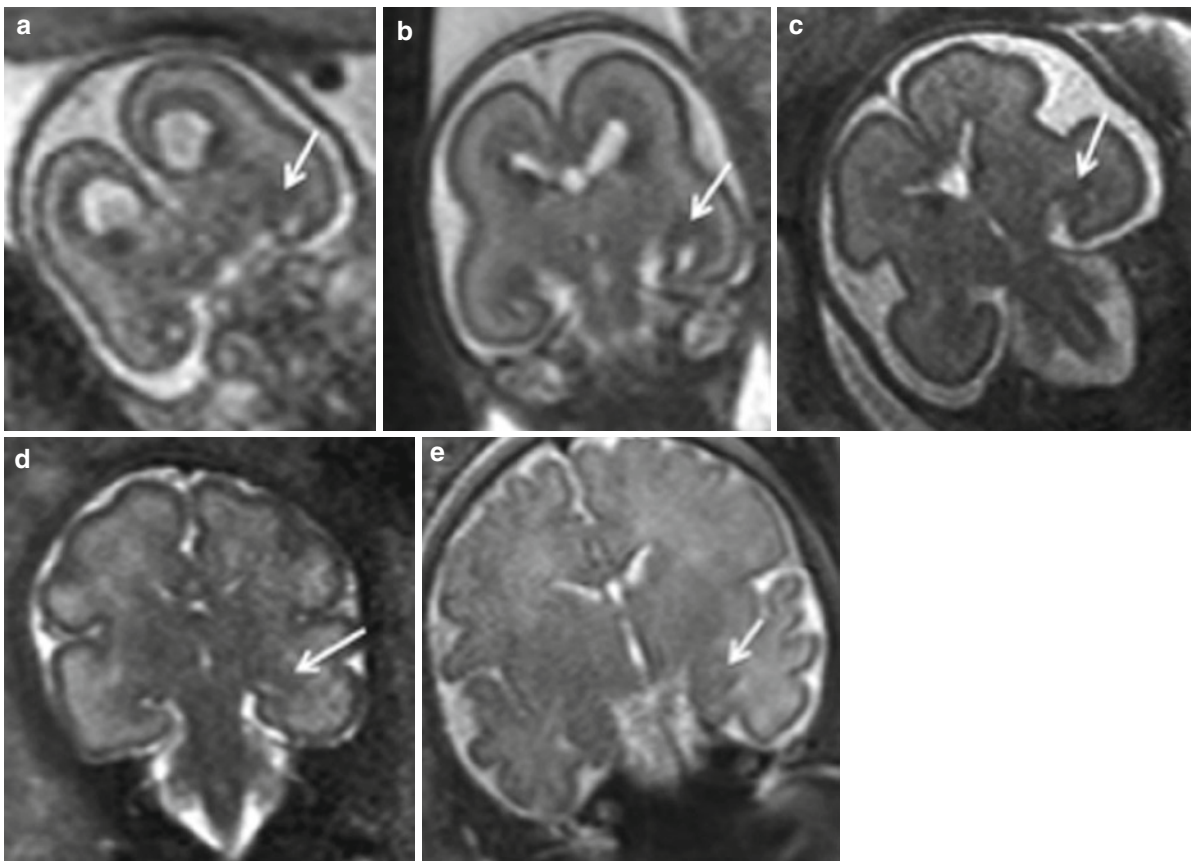

Fig. 8 Development of the hippocampus in coronal T2-weighted sequences of fetuses at (**a**) 18+1, (**b**) 20+4, (**c**) 24+3, (**d**) 31+1, and (**e**) 36+6. Note the hypointensity of the hippocampus and amygdaloid complex (*white arrows*). First the hippocampus shows a vertical position (S-shaped), and then it rotates and appears as a horizontal structure. Note also the development of the hippocampal sulcus (**c**–**e**)

At 15 GW, the hippocampus has the appearance of an upright "S" shape. Between 15 and 24 GW, there is cell proliferation and horizontal migration (Arnold and Trojanowski 1996). The vertical orientation of the hippocampus undergoes progressive rotation until 22–24 GW when it appears more horizontal and inferomedial position in the temporal horn. Subsequently, the volume of the hippocampus increases due to increased numbers of glial and endothelial cell components.

Fornical connections occur as early as 10–11 GW with the exchange of fibers across the midline (Raybaud 2010). In the third trimester, hippocampal fiber connections are established as the hippocampal network matures. Gamma-aminobutyric acid (GABA)ergic interneurons are thought to play an excitatory role in the maturation of the hippocampal network (Ben-Ari et al. 2004). Activity in the hippocampal or neocortical networks is present in late gestation in primates (Khazipov et al. 2001).

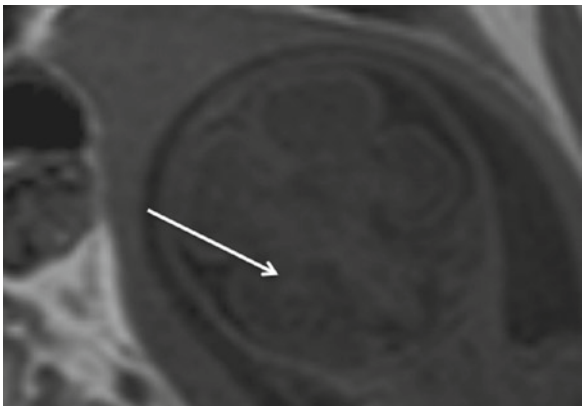

Fig. 9 Coronal T1-weighted sequence of a fetus (24+0 GW). The hippocampus appears as a hyperintense structure (*white arrow*)

4.1 MRI Findings of Temporal Lobe Development

In vitro, the hippocampus is a hypointense structure along the medial surface of the temporal lobe on T2W sequences, adjacent to the hippocampal sulcus (Kier et al. 1997) (Fig. 8). The hippocampus has a thick marginal zone, visible as a zone of T2W hyperintensity and low T1W intensity on postmortem images (Rados et al. 2006).

Coronal T2W images can provide information about hippocampal development in vivo (Kasprian 2006). At 18 GW, the hippocampus is hypointense and has a slim "S-shaped" appearance. The hippocampal sulcus appears as a deep horizontal indentation between the parahippocampal gyrus and the forming cornu ammonis (Prayer et al. 2006). (Fig. 8c–e). The medial border of the hippocampal sulcus fuses around 20 GW. The process may be incomplete and leave residual cysts (Bronen and Cheung 1991; Sasaki et al. 1993). Coronal T2W images between 20 and 24 GW demonstrate the growth and changing morphology of the hippocampus. Initially, the hippocampus is vertically oriented, and progressively becomes more horizontal by 22–24 GW (Fig. 8a–c). The degree of rotation of the hippocampus can be measured on fetal MR images by using the hippocampal infolding angle, which increases with gestational age (Righini et al. 2006). After 24 GW, the hippocampus appears as a horizontally oriented structure at the medial ventricular border of the temporal horn (Prayer et al. 2006) (Fig. 8d, e). Subsequently, the hippocampus increases in thickness and volume. Hyperintense signal is visible throughout all areas on axial T1W sequences (Fig. 9). This probably is a result of the increasing glial, endothelial, and neuronal cellularity (Prayer et al. 2006). A focal area of T2W hyperintensity develops in the temporopolar white matter around 28 GW (Prayer et al. 2006), correlating with the development of the amygdalocortical connections and temporal cortical plate (Fig. 8).

Gyration of the temporal lobe begins after 24 GW. The superior temporal sulcus serves as a landmark for gyral development and correlates well with gestational age in anatomical studies (Larroche 1981). At 25 GW, the posterior part of the superior temporal gyrus develops (Chi et al. 1977) (Fig. 10b), and by 32–34 GW, its formation is complete (Kasprian 2006). Concurrent with, or subsequent to, the appearance of the superior temporal gyrus, the collateral sulcus develops (Fig. 10a), and all primary sulci are visible by 34 GW (Garel et al. 2001).

The amygdaloid complex has a hypointense appearance rostral to the temporal horn of the lateral ventricle on coronal T2W images at 18 GW. The amygdala appears hyperintense on T1W images and persists through term. These signal intensities most likely result from cellularity (Prayer et al. 2006). At 1.5 T, T2W MR resolution is not adequate to delineate the hypointense

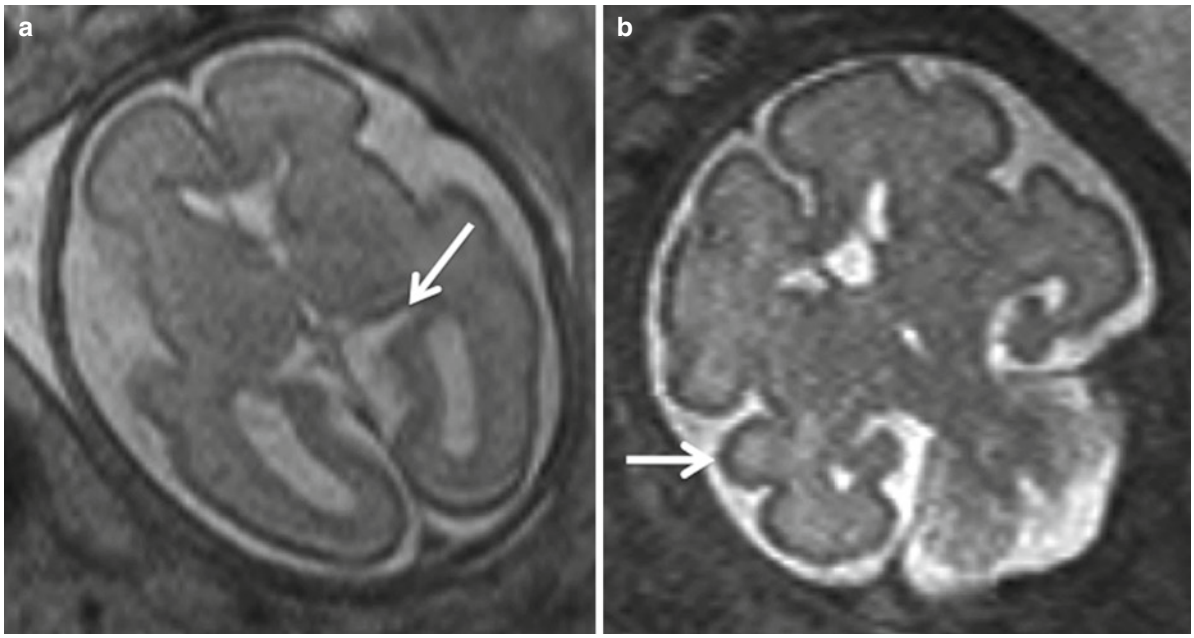

Fig. 10 T2-weighted sequences of fetuses at 24+4 GW (**a**) – axial; and at 25+4GW (**b**) – coronal. On the left image the collateral sulcus is visible (*white arrow*). On the right, the T2-weighted image shows the developing superior temporal gyrus (*white arrow*)

ganglionic eminence inferiorly. Before 31 GW, the amygdala, piriform cortex, and hippocampal head appear as a continuous zone of hypointensity in the medial temporopolar area on axial T2W sequences (Fig. 11). When formation of the anterior temporal lobe gyri begins at 31 GW, growth of the temporal lateral neocortex displaces this area more posteromedially within the temporal lobe (Prayer et al. 2006).

5 Transient Structures in the Fetal Brain

The appearances of transient structures in the fetal brain are critical steps in normal brain development. Transient structures include the subplate (as discussed above), the perireticular nucleus, the gangliothalamic body, and periventricular crossroads (Letinic and Kostovic 1997; Kostovic and Judas 1998; Ulfig 2000; Prayer et al. 2006).

The perireticular nucleus contains neurons that function as guideposts that direct corticothalamic fibers toward the dorsal thalamus and corticofugal fibers toward the brainstem (Ulfig 2000). Pioneer axons originate in the internal capsule and move to the thalamus, and may provide a framework for thalamocortical connections (Coleman and Mitrofanis 1999). The perireticular nucleus involutes due to cell

Fig. 11 Axial T2-weighted sequence of a fetus at 29+5 GW. Note the focal area of hyperintensity in the temporopolar white matter (*white arrow*). There is also a continuous zone of hypointensity in the medial temporopolar area which is formed by the amygdala, piriform cortex and hippocampal head before 31 GW (*black arrow*)

apoptosis or migration (Earle and Mitrofanis 1996) and displacement due to expansion of the fibers of the internal capsule (Tulay et al. 2004). The gangliothalamic body exists between 15 and 34 GW and represents a stream of migrating neurons between the ganglionic eminence and the pulvinar thalami. It regresses most likely as a result of cell migration (Letinic and Kostovic 1997).

Periventricular crossroads are special areas of periventricular white matter where growing fibers encounter axonal guidance molecules during growth. Crossroads result from a transiently increased content of extracellular matrix in association with radial and tangential migration of immature fibers (Judas et al. 2005). They are most prominent in the frontal lobe anterolateral to the frontal horn of the lateral ventricles.

5.1 MRI Findings of Transient Structures

The ganglionic eminence is visible on in vitro MRI scans at 10 GW (Brisse et al. 1997). The volume increases until about 26 GW, at which point it begins to diminish, persisting the longest in the superior ganglionic eminence (Kinoshita et al. 2001; Ulfig 2000). The gangliothalamic body is isointense to the adjacent gray matter nuclei and ganglionic eminence on MR images. Lack of DW anisotropy may be due to the nonlinear direction of the stream of migrating neurons (Prayer et al. 2006). The MRI appearances of periventricular crossroads will be discussed in the following sections.

6 White Matter Development

Prospective white matter develops from the second wave of postmitotic cells generated by cells in the ventricular zone. It appears between the ventricular zone and the marginal zone and therefore is termed the intermediate zone (Kostovic and Judas 2002; Samuelsen et al. 2003). The intermediate zone contains growing axonal pathways and oligodendrocyte progenitors. Neuronal migration and growth of axons take place principally in the intermediate zone (fetal white matter) and the subplate zone between the intermediate zone and the cortical plate (Rakic 2004). Growing thalamocortical fibers within transient zones and cortical afferent axons are distributed in the intermediate zone (fetal white matter). They also form an extensive system that involves the subplate zone and periventricular fiber-rich zone (Kostovic and Judas 2002; Judas et al. 2005). Collections of growing axons exhibit two morphological patterns: a laminar arrangement (Kostovic and Judas 2002) and periventricular crossroads (Judas et al. 2005). The cell number of the intermediate zone increases by a factor of 3.8 between 13 and 20 GW (Samuelsen et al. 2003). Since postmitotic neurons need several weeks to reach their final destination, as many as 30 generations of neurons can be simultaneously aligned along a single radial glial shaft within the wide intermediate zone (Rakic 2003). Tangential migration also occurs perpendicular to the radial glia (Menezes et al. 2002). A pathway for migration of callosal axons may also be provided by neurons at the

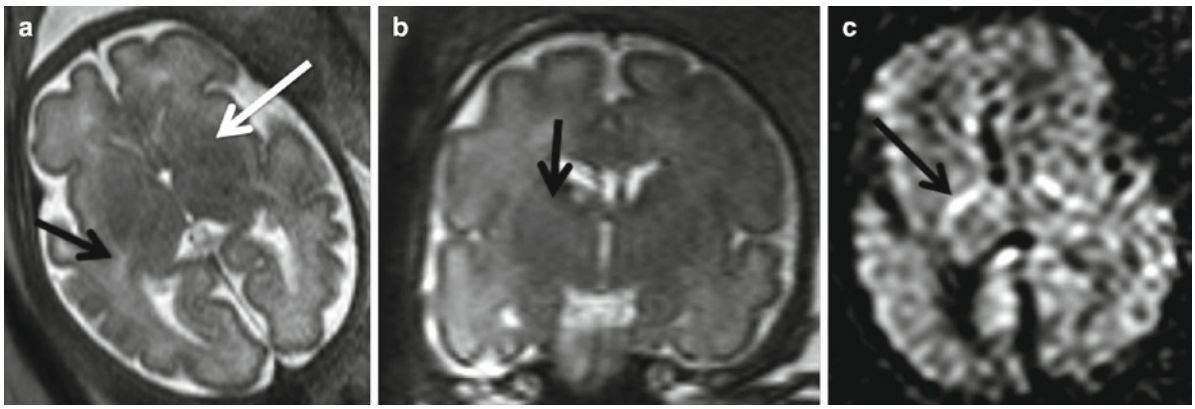

Fig. 12 Axial (**a**) and coronal (**b**) T2-weighted sequence of a fetus at 32+5. Note the hyperintensity of internal capsule (*black arrows*). A small lesion is present to the right of the arrow in image (**b**). The gray nuclei appear more hypointense on T2-weighted images in comparison to the internal capsule (*white arrow*). (**c**) Axial diffusion-weighted sequence of a fetus at 32+5 GW. Note the anisotropic posterior crus of the internal capsule that can be detected as early as 22 GW

border between the subventricular zone and the intermediate zone (Del Rio et al. 2000).

Fetal white matter development is also characterized by prominent areas of extracellular matrix in periventricular areas where there are numerous crossing fibers, known as periventricular crossroads (Judas et al. 2005). These areas of crossing efferent, afferent, associative, and callosal fibers are characterized by abundant hydrophilic extracellular matrix which contain axonal guidance material (see above). Originally described in preterm neonates (Battin et al. 1998), they have a "cap-like" appearance on MR images. Crossroads may also be identified adjacent to the caudal portion of the ganglionic eminence, lateral to the posterior crus of the internal capsule, and appear similar to those in the frontal and occipital region between 20 and 30 GW. Crossroads appear hypointense relative to white matter on T1W images and hyperintense on T2W images, and are seen in the frontal and occipital white matter. They become visible around 24 GW and persist throughout gestation. These are visible on fetal MR images by about 22 GW, and are "slightly hyperintense" on T2W images and "slightly hypointense" on T1W images relative to the intermediate zone (Kostovic and Judas 2002). These have been described in six locations: the main crossroad at the lateral margin of the frontal horn and body of the lateral ventricle, the frontal crossroad along the dorsal aspect of the lateral ventricle, a frontal crossroad inferolateral to the frontal horn and ventral to the putamen, the occipital crossroad lateral to the atrium and occipital horn, the parietal crossroad anterolateral to the atrium and centered over the retrolenticular internal capsule (the "Wetterwinkel" (Prayer et al. 2005) (Fig. 13), and the temporal crossroad anterolateral to the temporal horn (Judas et al. 2005) (Fig. 11).

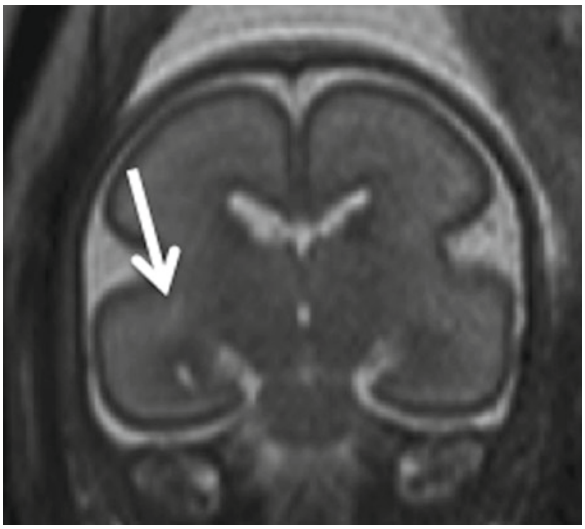

Fig. 13 Coronal T2-weighted sequence of a fetus at 23+0 GW. Crossroads appear hypointense relative to white matter on T1W images and hyperintense on T2W images. Note the triangular crossroad the so-called Wetterwinkel (*white arrow*)

6.1 White Matter Tract Formation

Neural connectivity depends on the directed growth of axons (Richards et al. 1997). The internal capsule is visible in the late embryonic period at the time of preplate formation, and is shaped by emerging thalamic axons (Molnar and Blakemore 1995; O'Rahilly and Muller 1999). However, before 20 GW it is a potential space that contains undifferentiated blast cells (Tulay et al. 2004). The axons that form the internal capsule are mainly derived from the subplate (Koester and O'Leary 1994). At 12–15 GW, three fiber systems are visible: the corpus callosum, the fornix, and the cerebral stalk, which contains all the projection fibers of the developing internal capsule including thalamocortical fibers (Rados et al. 2006).

Axons that form the pyramidal tracts in the late embryonic period also come from the subplate (ten Donkelaar 2000). Decussation of the pyramidal tract is complete by 17 GW, myelination is present at 25 GW, and corticospinal tract fibers reach the spinal cord by 24 GW (Eyre et al. 2000).

From 17 to 24 GW, the corpus callosum, the fornix, the internal capsule, and the external capsule continue to grow and develop. The growing fiber tracts intersect at the periventricular crossroads (Judas et al. 2005). From 24 to 32 GW, the corona radiata develops, and all major segments of the cerebral white matter can be identified (Kostovic and Judas 2002). These include the corpus callosum, the peduncular part of the corona radiata, the centrum semiovale, and gyral white matter. Between 32 weeks and term, the internal capsule becomes well-defined due to the onset of myelination. Gyral white matter becomes well-developed.

Myelination occurs predominantly postnatally (Counsell et al. 2002) in a craniocaudad and centrifugal fashion (Garel et al. 2003; Kinney 2005). Although there is evidence of myelination in the spinal cord as early as

15–21 GW (Grever et al. 1996), the first histological evidence of brain myelination occurs at 21 GW in the brainstem and internal capsule (Shiraishi et al. 2003) and in the thalamus at 22 GW (Jakovcevski and Zecevic 2005). The number of immature oligodendrocytes increases about 3 months prior to the onset of myelination, referred to as myelination gliosis (Girard et al. 1991). At 20 GW, premyelination changes occur when oligodendrocyte progenitors transform into oligodendrocytes. There are three phases of myelination: "premyelin sheath" formation by immature oligodendrocytes; formation of a "transitional sheath," which contains myelin basic protein which is characteristic of mature myelin; and formation of a mature myelin sheath, which contains myelin basic protein (Back et al. 2002).

6.2 MRI of White Matter Development

On T1W postmortem MR images, the subplate has lower signal intensity than the intermediate zone. Postmortem and T2W images display higher signal intensity in the subplate compared with the intermediate zone. This correlates with histological changes of decreased extracellular matrix and increased cellularity in the subplate layer. Antenatal T2W images show similar findings (Widjaja et al. 2010b). On DW sequences, there is no anisotropy due to microstructural changes of the differing fiber pathways across the zones (Prayer et al. 2006; Widjaja et al. 2010a). After 27 GW, water content in the subplate decreases, and the interface between the intermediate zone and the subplate becomes less distinct. In vivo, the internal capsule is hyperintense on T2W images and hypointense relative to the basal ganglia on T1W images. After 28 GW in the preterm neonate (Counsell et al. 2002) and 30th week in the fetal brain (Garel et al. 2003), the posterior limb of the internal capsule becomes T2W hypointense and T1W hyperintense (Fig. 12a, b). DW anisotropy can be detected in the posterior crus as early as 22 GW (Prayer et al. 2006) (Fig. 12c). In preterm neonate brains, the posterior crus shows lower mean diffusivity and higher fractional anisotropy than other unmyelinated white matter tracts (Partridge et al. 2004). Signal changes can be ascribed to increased cell density related to the perireticular nucleus neurons and glial cells or due to alignment of the neurons, creating an asymmetrical environment (Prayer et al. 2006).

Premyelinating changes in the corticospinal tract, the longitudinal fasciculus at the level of the brainstem, the internal capsule, the CC, and the optic chiasm can be recognized on DW imaging (Wimberger et al. 1995; Prayer and Prayer 2003; Partridge et al. 2004) (Fig. 14). White matter tract anisotropy precedes myelination, probably due to histological changes as the axons develop and tracts mature, and to the establishment of an axon potential (Huppi et al. 1998) which promotes differentiation of immature oligodendrocytes and stimulates myelination (Fields 2004).

The technique of diffusion tensor imaging (DTI), by measuring the directionality of diffusion, allows a three-dimensional reconstruction of tissue microstructure and thus can depict the architecture of the developing fetal brain (Le Bihan et al. 1986). The DTI technique has been used to study and quantify white matter maturation and development (Huppi et al. 1998; Childs et al. 2001; Mukherjee et al. 2002; Zhai et al. 2003; Maas et al. 2004; Partridge et al. 2004; Berman et al. 2005; Partridge et al. 2005; Yoo et al. 2005; Bui et al. 2006; Huang et al. 2006; Anjari et al. 2007; Dubois et al. 2008). DTI sequence optimization permits the in utero acquisition of data on unsedated fetuses, allowing visualization of corticospinal and callosal pathways in 40% of cases (Kasprian et al. 2008) (Fig. 15). DTI detects regions of intermingling callosal and craniocaudal pathways anterolaterally to the anterior horns of the lateral ventricles. These correlate with the periventricular "caps" (Battin 2001) seen on T2W images which correspond with the periventricular crossroads described both histologically and on postmortem studies.

7 Development of the Corpus Callosum

At 10 GW, the interhemispheric fissure contains meninx primitiva, and deepens, resulting in a cleft in the dorsal lamina reuniens and formation of the sulcus medianus telencephali medii (Rakic and Yakovlev 1968). The sulci are close together at the edge of the cortical plate (Rakic and Yakovlev 1968) at the corticoseptal boundary which is genetically predetermined (Hankin and Silver 1988; Shu and Richards 2001; Shu et al. 2003; Richards et al. 2004; Shen et al. 2006). A glial sling is formed by medial migration of glial and possibly neuronal cells from

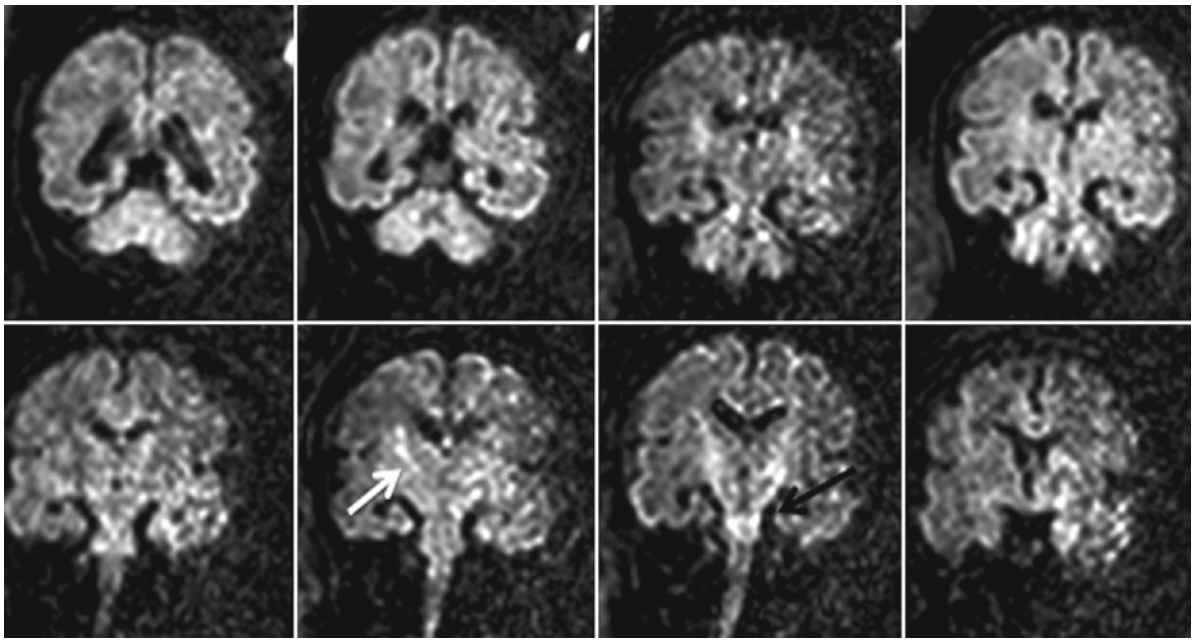

Fig. 14 Premyelinating changes can be recognized on coronal diffusion-weighted images at GW 34+0. Note the anisotropy of the internal capsule (*white arrow*) and of the longitudinal fasciculus at the level of the brainstem

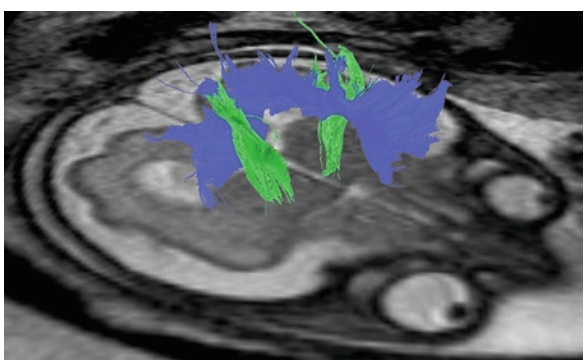

Fig. 15 Diffusion tensor imaging sequence optimization allows the in utero acquisition of data on unsedated fetuses, allowing visualization of corticospinal and callosal pathways at GW 28+2

the subventricular zone toward the midline at around 12 GW (Rakic and Yakovlev 1968; Silver et al. 1982; Katz et al. 1983; Hankin and Silver 1988; Shu and Richards 2001; Shu et al. 2003; Richards et al. 2004) (Lent et al. 2005; Ren et al. 2006). The glial sling forms an interhemispheric bridge that supports the crossing of the first pioneer axons at 12–13 GW (Rakic and Yakovlev 1968). If the glial sling is not present, the callosal fibers do not cross and instead extend parallel to the midline (Silver et al. 1982). Further guidance of axons across the midline is provided by two other glial structures: the indusium griseum and the glial wedge (Shu and Richards 2001; Richards 2002; Shu et al. 2003; Richards et al. 2004). These structures repel pioneer axons initially from the cingulate cortex (Koester and O'Leary 1994; Richards 2002) and direct them toward the glial sling and the midline. Axons are guided across the midline to homologous regions in the contralateral hemisphere by a variety of guidance molecules, transcription factors, and morphogens that are chemoattractive and chemorepulsive (Richards et al. 1997; Richards 2002; Judas et al. 2005; Plachez and Richards 2005; Shen et al. 2006; Lindwall et al. 2007). Subsequently, neocortical axons join them in a process that occurs within GW 13 (Rakic and Yakovlev 1968). Neocortical commisural axons from the anterior hemisphere arrive by means of the pioneer callosal fibers and the glial sling, while those from the posterior neocortex cross along the hippocampal commissure (Raybaud 2010). Both anterior and posterior sections continue to grow and fuse and all parts of the corpus callosum are fused and complete by GW 14 or 15 (Kier and Truwit 1996, 1997). At this point, the corpus callosum is short but grows by addition of fibers as the cortex develops and connectivity increases until after birth (Raybaud 2010). Rather than developing from front

to back as has been postulated, it appears that in humans, due to disproportionate growth of the frontal lobes, there is a corresponding increase in anterior callosal fibers (Huang et al. 2009). This causes the splenium and hippocampal fissure to be shifted posteriorly into position above the posterior third ventricle and tectal plate (Raybaud 2010).

The splenium of the corpus callosum becomes prominent by 18–19 GW (Ren et al. 2006) and the overall shape of the corpus callosum is established by GW 20 (Raybaud 2010). At this stage the cross-sectional area is only 5% of that of a 5-year-old child, and in neonatal life prior to myelinization is 50% of the size (Huang et al. 2006; Jovanov-Milosevic et al. 2009). The corpus callosum enlarges in a proportional fashion to the cortical growth and complexity in utero by the addition of fibers (Raybaud 2010).

7.1 MRI of Development of the Corpus Callosum

The corpus callosum is seen on T2W images in the midline sagittal plane as a horizontal thin curvilinear C-shaped hypointense structure (relative to the subplate) at the superior margin of the cavum septi pellucidi (Fig. 16a). It increases in length and thickness with gestational age. Normative values for callosal length are available (Garel 2004; Parazzini et al. 2008; Chung et al. 2009; Tilea et al. 2009). Diffusion tensor imaging with fiber-tracking has been used to demonstrate callosal fibers and trajectories (Kasprian et al. 2008) (Fig. 16b).

8 Normal Development of the Ventricular System

The ventricular walls are composed of cells of the ventricular zone (germinal matrix). It is the innermost layer of the developing cerebral cortex. It is thickest early in gestation, regressing in the third trimester(Fig. 2). A single layer of ependymal cells lines the ventricular walls by 28 GW. Germinal matrix cells persist in the roof of the temporal horn and in the occipital horn lateral wall until 33 GW, and persist later in the caudothalamic groove (Kinoshita et al. 2001; Bystron et al. 2008).

8.1 MRI of the Ventricular System

The ventricular zone is visible on MR images as a dark band on T2W sequences and a bright band on T1W sequences (Fig. 3a–d). The diameter of the atria of the lateral ventricles remains constant from 15 to 35 GW, but particularly on MR images, appears more prominent

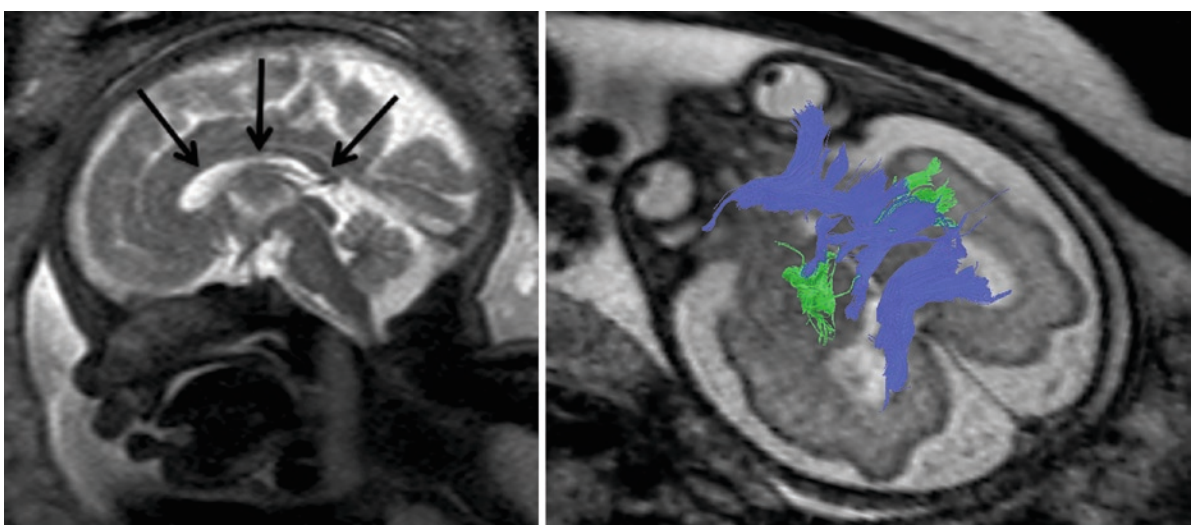

Fig. 16 (**a**) Sagittal T2-weighted sequence of a fetus at GW 32. The corpus callosum can be identified as a horizontal thin C-shaped hypointense structure (*black arrows*). (**b**) Diffusion tensor imaging with fiber-tracking at 28+2 GW can be used to demonstrate callosal fibers and trajectories

in early gestation due to the relative paucity of brain parenchyma relative to ventricular size at early gestational ages (Prayer et al. 2006) (Fig. 2). Sonographic studies have reported mean atrial diameters in the axial plane of 5.4–7.6 mm at the posterior margin of the glomus in the axial plane (Cardoza and Filly 1988; Alagappan et al. 1994; Filly and Goldstein 1994). Normative values have been reported using MRI, and mean values are comparable to sonographic studies (Levine et al. 2002; Twickler et al. 2002; Parazzini et al. 2008; Chung et al. 2009). However, the normal range of ventricular measurements is considerably more variable and may be significantly greater with MRI in the axial plane between 18 and 25 GW. Measurements in normal fetuses in this age group may exceed the normal sonographic upper limit of 10 mm, most likely related to artifacts related to motion, slice thickness, pulse sequences, screen pixels, and small size of target objects (Chung et al. 2009). In the coronal plane, at a median gestational age of 32 GW, sonographic and MRI ventricular measurements were shown to correlate well (Garel and Alberti 2006). The cavum septi pellucidi is visible until fusion of the septal leaves occurs near birth (Fig. 17).

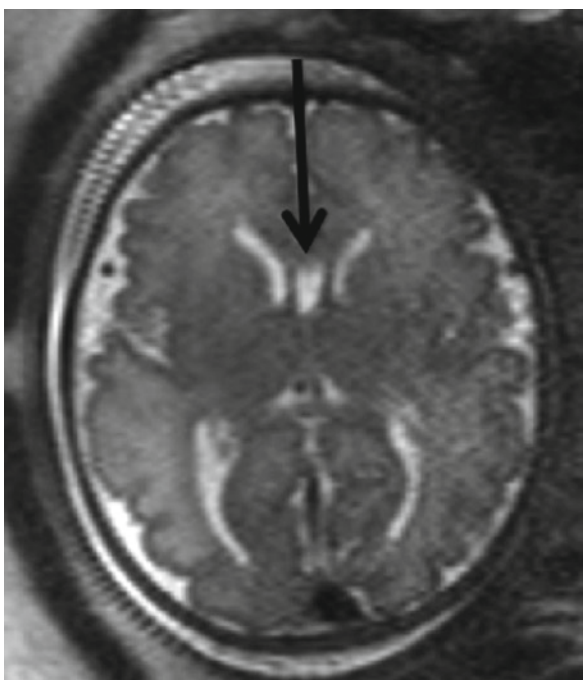

Fig. 17 Axial T2-weighted sequence of a fetus at 35+1 GW. The image shows cavum septi pellucidi that is visible until the fusion of the septi near term

9 Development of the Deep Gray Nuclei

During the embryonic period, the striatum (caudate and putamen) and globus pallidus arise from the medial and lateral ganglionic eminences that represent the germinal matrix areas of the ventral forebrain (Marin and Rubenstein 2003). Thalamic cells are derived from the germinal matrix lining the diencephalon (Rakic and Yakovlev 1968; Kostovic 1990; Petanjek et al. 2008). Between 17 and 37 GW, thalamic cells are derived from the gangliothalamic body, which extends from the ganglionic eminence to the thalamus. The gangliothalamic body is the source of gamma-aminobutyric acid–producing cells that migrate tangentially to the thalamus (Letinic and Rakic 2001; Petanjek et al. 2008).

9.1 MRI Findings of the Deep Gray Nuclei Development

Early in gestation, the deep gray nuclei are isointense to slightly hypointense relative to white matter on T2W sequences. After 28 GW, they appear more hyperintense on T1W sequences (Garel 2004) and more hypointense on T2W images relative to the internal capsule (Fig. 12) (Lan et al. 2000). Diffusion-weighted images show a decline in mean diffusivity in the basal ganglia and thalamus with advancing gestational age (Righini et al. 2003; Manganaro et al. 2007; Schneider et al. 2007, 2009). In addition, the pituitary stalk can be detected on axial, coronal, or sagittal T2W images beginning at 16 GW (Righini et al. 2009; Schmook et al. 2010) (Fig. 18). The pituitary gland can be detected on T1W sequences after 16 GW, with the detection rate and size increasing with gestational age (Schmook et al. 2010).

10 Cerebellar Development

Cerebellar development begins in the fifth to sixth GW, and continues after birth (ten Donkelaar et al. 2003; ten Donkelaar and Lammens 2009). Maturation of the cerebellum occurs later than that of the telencephalon (Simonati et al. 1999). The initial phase of cerebellar development consists of differentiation from the hindbrain as it originates from the metencephalon (rhombencephalon) and mesencephalon (midbrain). The pontine

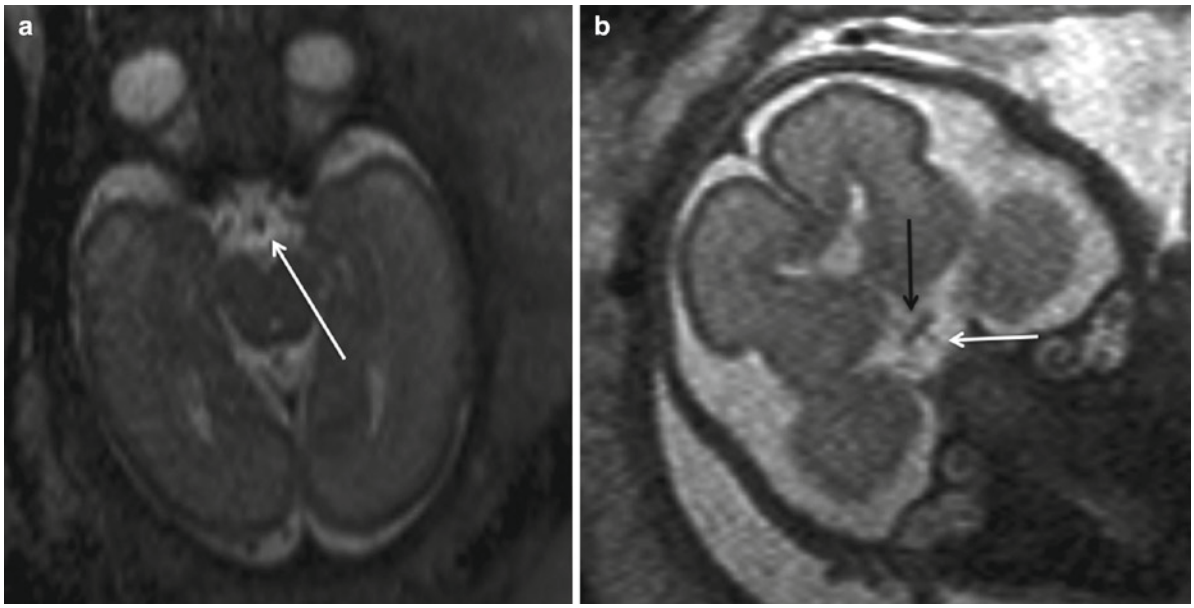

Fig. 18 (**a**) Axial and (**b**) coronal T2-weighted sequences of a fetus at 24+0 GW. The pituitary stalk (*white arrows*) can be seen on T2-weighted images beginning at 16 GW as well as the optic chiasm (*black arrow*)

flexure develops at the same time as the cerebellar hemispheres (Nakayama and Yamada 1999). The isthmic organizer, a region in the caudal mesencephalon, is situated at the border between the midbrain and hind-brain, and coordinates development of the cerebellum and pons (Nakayama and Yamada 1999; Basson et al. 2008). Initial development of the cerebellum is from neuroepithelial cells in the ventricular zone (Larroche 1981).

The second cerebellar developmental phase is cell production in two germinal matrix zones that disappear after birth which are believed to be the source of cerebellar neurons, the ventricular zone, and the rhombic lips (Hynes et al. 1986). The first region is the ventricular zone in the roof of the fourth ventricle, from which originate initially Purkinje cells and deep cerebellar neurons, and subsequently basket cells, stellate cells, and Golgi cells (ten Donkelaar et al. 2003; Sotelo 2004). Cells migrate from the ventricular zone toward the sparsely cellular outer marginal layer to form the intermediate zone at 5–10 GW (Larroche 1981). The internal granular layer develops by migration in a radial fashion (Hynes et al. 1986). The external granular layer, the second germinal zone develops between the 9th and 13th GW and originates by means of tangential migration from the rhombic lips (Larroche 1981) which are more dorsolaterally located in the metencephalon between the roof plate and the dorsal neuroepithelium at the caudal aspect of the fourth ventricle (Sotelo 2004). The rostral rhombic lip neuroepithelium gives rise to migrating cells which begin to move to the surface at 11–13 GW in a second wave, which becomes the granule cell layer after birth (Hynes et al. 1986). Pontine nuclei and the inferior olivary nucleus arise from the caudal portion (Nakayama and Yamada 1999; Sotelo 2004).

The third phase of cerebellar development begins in the 16th GW and involves inward migration of the granule cells, which persists throughout fetal life (Nakayama and Yamada 1999; ten Donkelaar et al. 2003).

The lamina dissecans is visible between 20 and 32 GW as a transient zone of migrating cells (Sidman and Rakic 1973; Nakayama and Yamada 1999). It separates the external granular cell layer from the deep internal granular cell layer (Larroche 1981; Abraham et al. 2001). The highest rate of proliferation occurs in this zone between 28 and 34 GW (Abraham et al. 2001). The lamina dissecans disappears from the flocculus and subsequently from the hemispheres while the Purkinje cell layer becomes more prominent along the outer surface of the lamina dissecans as it disappears. Postnatally, the external granular layer disappears around 10 months of age, leaving three layers of cerebellar cortex (Larroche 1981).

In the fourth phase of cerebellar development, there is further cell differentiation and development of neuronal circuits and cerebellar function (ten Donkelaar et al. 2003).

Anatomically, the first area to form is the flocculonodular lobe (Adamsbaum et al. 2005) and the first fissure to appear is the posterolateral fissure at 12–13 GW. The primary fissure develops at 14–15 GW, and is deepest in the midline. Prepyramidal, preculminate, and precentral fissures are seen at 15–16 GW. The horizontal fissure is visible by 21 GW (Adamsbaum et al. 2005). Foliation of the vermis begins at 14 GW. The deep gray matter nuclei of the cerebellum originate from the ventricular zone. The dentate nuclei may be detected by 11 GW (Yamaguchi and Goto 1997) to 16 GW (Mihajlovic and Zecevic 1986). The vermis is formed at the time of the fusion of the cerebellar hemispheres at the end of the 8th GW. The cerebellar hemispheres grow faster than the vermis and attain a mature morphology by 22 GW.

10.1 MRI of Cerebellar Development

The small size of cerebellar structures precludes early visualization of some structures and therefore MR appearances are delayed relative to histological development. In vitro MR can demonstrate the rhombencephalic vesicle (primitive fourth ventricle) after 10 GW (Chong et al. 1997). The transverse cerebellar diameter increases during gestation and can be measured using fetal MRI (Chung et al. 2009). Vermian normative biometric data are also available (Garel et al. 2003; Triulzi et al. 2005; Parazzini et al. 2008; Tilea et al. 2009). The fetal cerebellum has an extremely high cell density and therefore appears hypointense on T2W, hyperintense on T1W, and bright on diffusion-weighted images (Fig. 19). The lack of anisotropy is probably due to the different direction of migrating neuronal pathways (Prayer and Prayer 2003; Prayer et al. 2006) (Fig. 20). Mean diffusivity decreases with gestational age (Schneider et al. 2007, 2009). The hemispheres appear multilayered after 20 GW (Fig. 20). T2 hypointensity and T1 hyperintensity in the central area represent deep gray nuclei surrounded by T2 hyperintense tissue with T2 hypointense cortex which includes the deep granular layer (Chong et al. 1997; Adamsbaum et al. 2005; Triulzi et al. 2005) (Fig. 21). T2 hypointensity deep in the cerebellar hemispheres has been attributed to the cell-dense dentate nucleus and is best seen on sagittal images from 21 GW (Adamsbaum et al. 2005). Gyration of the dentate nucleus, after 30 GW, is hypointense on T2W images, relative to the hyperintense core (Prayer et al. 2006) (Fig. 19b, c).

The vermis encloses the fourth ventricle by 20 GW (Adamsbaum et al. 2005). The vermis is optimally assessed on thin midline sagittal T2W sections as well as axial and coronal planes. The primary fissure is visible on midline sagittal images by 25–26 GW and beginning as early as 20–21 GW (Fig. 16), with other fissures appearing subsequently (Figs. 16 and 24). Optimal image quality is critical to their visibility (Adamsbaum et al. 2005). The distal tips of the cerebellar foliae are focally hypointense on T2W images, which could be due to a higher density of Purkinje cells in the periphery (Isumi et al. 1997) (Fig. 21). Vermian foliae can be differentiated on T2W images at 24 GW and hemispheric foliae by 30 GW (Triulzi et al. 2005) (Fig. 22). The flocculonodular lobule is hypointense on T2W images by 30–31 GW (Triulzi et al. 2005) (Fig. 23).

11 Brainstem Development

The brainstem forms between 6 and 7 GW and matures in a caudal to rostral direction. The medulla develops from the myelencephalon and develops and functions earlier than the pons and midbrain (Joseph 2000). The brainstem continues to develop throughout gestation and continues postnatally until about 6 months after birth. Descending motor tracts as well as the nuclei of cranial nerves VIII–XII are located within the medulla. The nucleus of the solitary tract is located in the dorsal aspect of the medulla and has a craniocaudad orientation.

11.1 MRI Appearance of Brainstem Development

Both the nucleus of the solitary tract and the corticospinal tract are visible after 18 GW. On T2W images, the ascending sensory tracts are hypointense due to cell density and myelination (Prayer et al. 2006). The pyramidal tract is relatively hyperintense. Both tracts are not sufficiently different in contrast on T1-weighted images to be visualized. The inferior cerebellar peduncles are hypointense on T2W images after 32 GW (Triulzi et al. 2005). However, on diffusion-weighted images, both structures demonstrate anisotropy (Fig. 27).

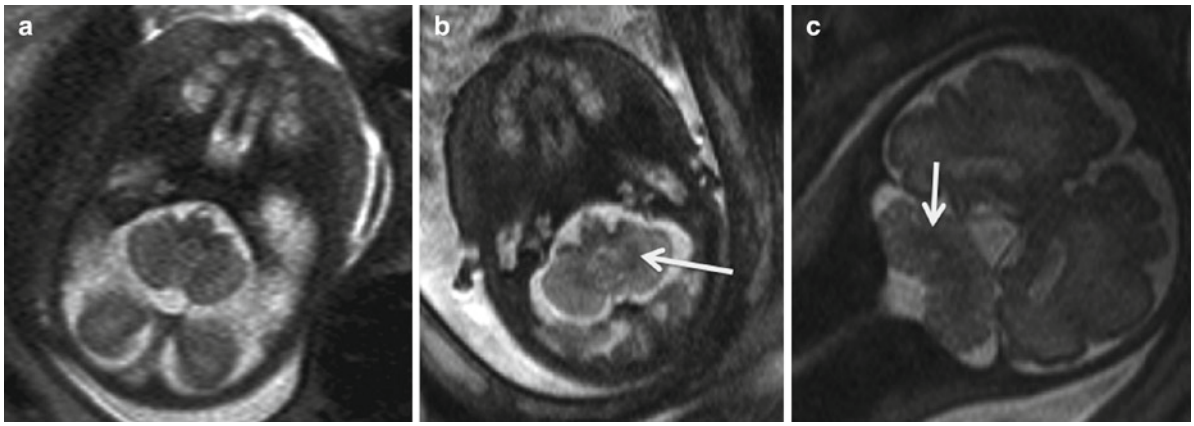

Fig. 19 (**a**) Axial T2-weighted sequence of a fetus at 28 GW. The cerebellar hemispheres appear multilayered. Axial T2-weighted sequence (**b**) and coronal T2-weighted sequence (**c**) of fetuses at 32+4 and 32+5GW. The gyration of the dentate nucleus shows hypointensity compared to the hyperintense core (*white arrow*)

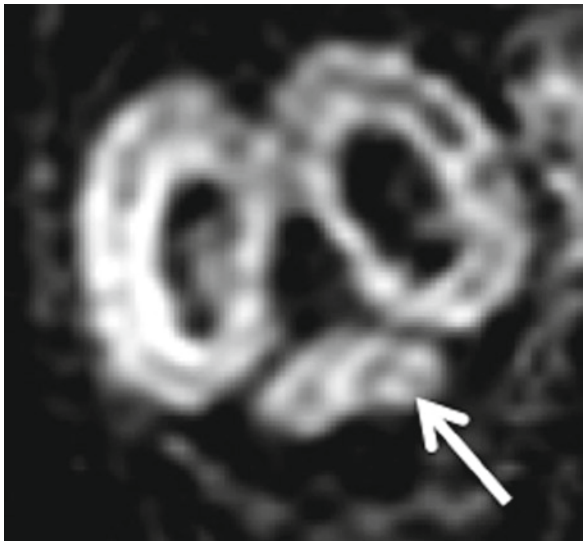

Fig. 20 Coronal diffusion-weighted sequence of a fetus at 20+4 GW. The cerebellum appears isotropic on diffusion-weighted images. The lack of anisotropy is probably due to the different directions of migrating neuronal pathways

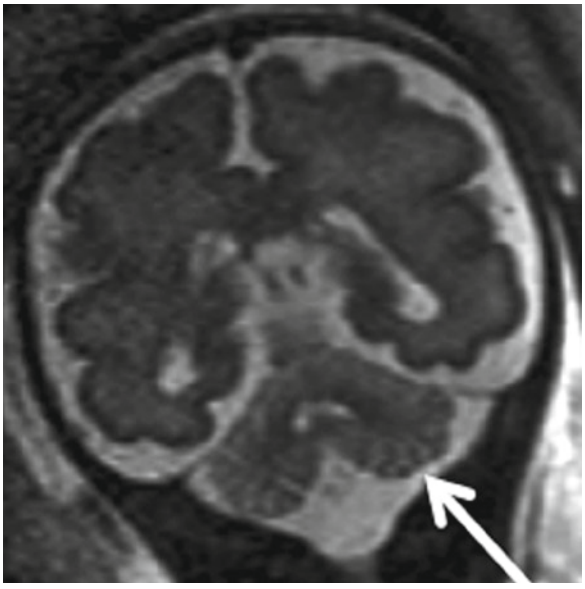

Fig. 21 Coronal T2-weighted sequence of a fetus at 26+0 GW. The distal tips of the cerebellar foliae are focally hypointense on T2-weighted images, which could be due to a higher density of Purkinje cells in the periphery

12 Development of the Pons

The pons develops after the medulla at around 8 GW (Joseph 2000). Structures within the pons include the nuclei of cranial nerves V–VIII, the tegmentum, the raphe nucleus, the locus coeruleus, and the medial longitudinal fasciculus. Pontine functions such as reactivity to acoustic and vibratory stimulation begin to develop after 26 GW (Joseph 2000).

12.1 MRI of Development of the Pons

The dorsal part of the pons is hypointense on T2W and hyperintense on T1W images after 24 GW (Girard et al. 1995; Adamsbaum et al. 2005; Triulzi et al. 2005) (Fig. 24). The ventral part maintains hyperintensity on T2W and hypointensity on T1W images until birth (Chong et al. 1997; Counsell et al.

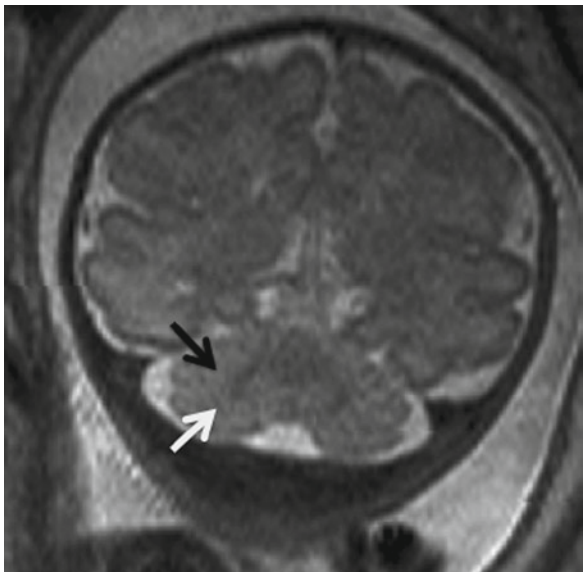

Fig. 22 Coronal T2-weighted of a fetus at 34+1 GW. The foliae of the cerebellar hemispheres can be discriminated, as well as the anterior lobe (*black arrow*) and posterior lobe (*white arrow*)

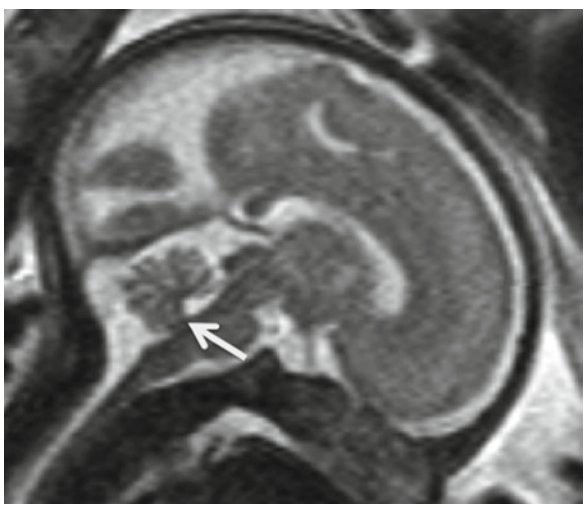

Fig. 23 Sagittal T2-weighted sequence of a fetus at 28+5 GW. The flocculonodular lobe can be identified because of its hypointensity (*white arrow*)

2002). On DW images, the pons is homogeneously hyperintense with no anisotropy (Prayer et al. 2006). Mean diffusivity of the pons decreases with increasing gestational age (Schneider et al. 2007; Schneider et al. 2009).

Fig. 24 Sagittal T2-weighted sequence of a fetus at 24+0 GW. Note the hypointensity of the dorsal part of the pons (*white arrow*)

13 Development of the Midbrain

The midbrain contains the substantia nigra, the inferior and superior colliculi, nuclei of cranial nerves III–VI, and the continuation of pontine structures (Joseph 2000). Auditory pathways develop and mature in fetal life with early maturation in the inferior colliculi, which are a "relay station" for auditory stimuli. After 18 GW, development in the inferior colliculi accelerates, then slows after 33 GW as Nissl bodies mature (Nara et al. 1996).

13.1 MRI of Development of the Midbrain

The inferior colliculi appear hypointense on T2W images as early 16 GW and reliably after 20 GW but are not seen well on other sequences due to their small size (Fig. 25). The dorsal midbrain appears hypointense on T2W and hyperintense on T1W images after 34 GW (Girard et al. 1995; Stazzone

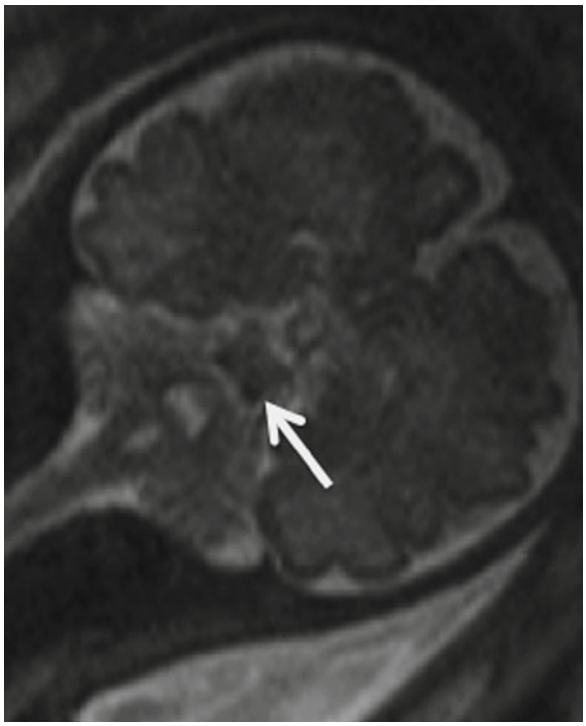

Fig. 25 Coronal T2-weighted sequence of a fetus (32+4 GW). The inferior colliculi appear hypointense (*white arrow*). They cannot be seen well on other sequences because of their small size

Fig. 26 Axial T2-weighted sequence of a fetus at 32+4 GW. The dorsal midbrain appears hypointense in T2W sequences with advanced gestational age (*black arrow*)

et al. 2000) (Fig. 26). Myelination begins between 20 and 24 GW. By 28 GW, the inferior and superior cerebellar peduncles appear as hypointense structures on T2W images (Fig. 27a), and anisotropic on DW sequences (Prayer et al. 2006) (Fig. 27b).

14 Fetal Behavior

Evaluation of behavior is a potentially useful indicator of normal CNS development and potential pathology, since fetal movement requires appropriate neuromuscular development and metabolism (Sparling et al. 1999; Olesen and Svare 2004). Further discussion of fetal behavior can be found in the chapter "Phylogeny and Ontogeny of Early Fetal Behavior" by Einspieler and Prechtl.

14.1 MRI and Fetal Behavior

Fetal movement can be documented using dynamic MR sequences (Prayer et al. 2006). Sequences of 30 s length can be obtained during a scan of 30–45 min and allow assessment of fetal behavior (Fig. 28). However, due to the short duration of observation, it is not possible to conclude definitively that fetal movement is absent, or to confirm reliably that abnormal behavior is present (Prayer et al. 2006).

15 Conclusion

Normal brain development can be assessed with MRI both morphologically as well as functionally in terms of fetal movement. In order to assess processes that interfere with developmental steps and the morphological changes that result from them, it is essential to first understand and recognize and interpret the normal developmental stages and to be familiar with MR appearances of normal brain development including the appearance and disappearance of transient structures.

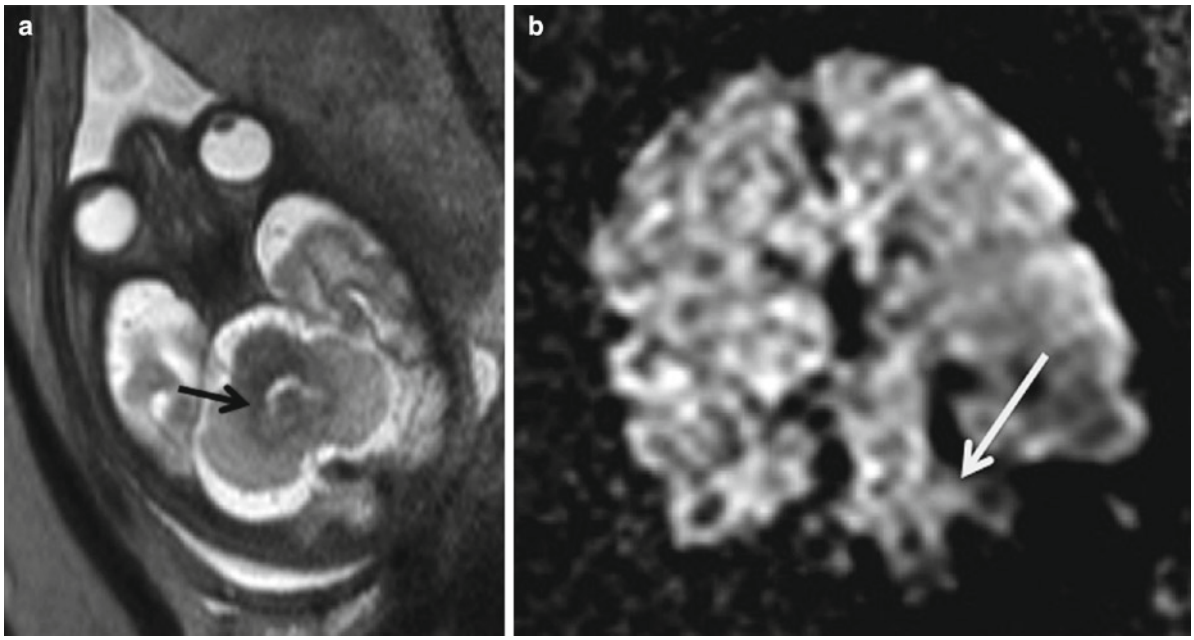

Fig. 27 (**a**) Axial T2-weighted sequence of a fetus (32+5 GW). At 28 GW, the inferior and superior cerebellar peduncles appear hypointense (*black arrow*) relative to the cerebellar hemispheres. (**b**) Coronal diffusion-weighted sequence of a fetus at 36+6 GW. The inferior cerebellar peduncles appear anisotropic (*white arrow*) whereas they are hypointense on T2-weighted images

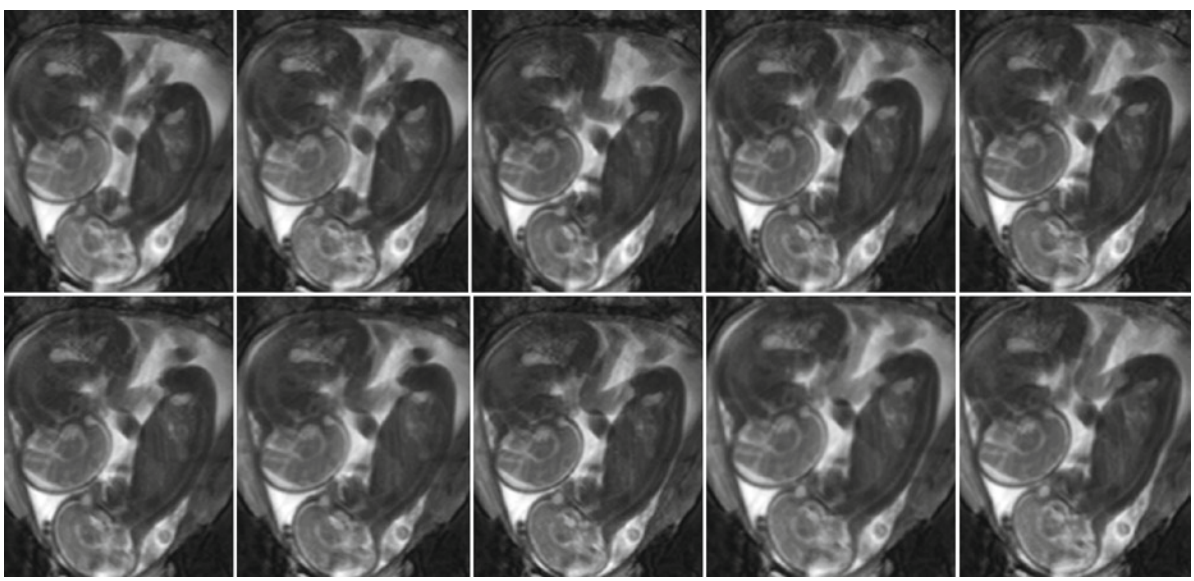

Fig. 28 Dynamic sequence of twins at 28+5 GW. Random movement of the limbs, swallowing and tongue movement is detectable. "Mouthing" is thought to be essential to motor speech development

References

Abraham H, Tornoczky T et al (2001) Cell formation in the cortical layers of the developing human cerebellum. Int J Dev Neurosci 19(1):53–62

Adamsbaum C, Moutard ML et al (2005) MRI of the fetal posterior fossa. Pediatr Radiol 35(2):124–140

Alagappan R, Browning PD et al (1994) Distal lateral ventricular atrium: reevaluation of normal range. Radiology 193(2): 405–408

Anjari M, Srinivasan L et al (2007) Diffusion tensor imaging with tract-based spatial statistics reveals local white matter abnormalities in preterm infants. Neuroimage 35(3):1021–1027

Arber S (2004) Subplate neurons: bridging the gap to function in the cortex. Trends Neurosci 27(3):111–113

Arnold SE, Trojanowski JQ (1996) Human fetal hippocampal development: I. Cytoarchitecture, myeloarchitecture, and neuronal morphologic features. J Comp Neurol 367(2): 274–292

Back SA, Luo NL et al (2002) Arrested oligodendrocyte lineage progression during human cerebral white matter development: dissociation between the timing of progenitor differentiation and myelinogenesis. J Neuropathol Exp Neurol 61(2):197–211

Ballabh P, Braun A et al (2004) Anatomic analysis of blood vessels in germinal matrix, cerebral cortex, and white matter in developing infants. Pediatr Res 56(1):117–124

Barkovich AJ, Kjos BO et al (1988) Normal maturation of the neonatal and infant brain: MR imaging at 1.5 T. Radiology 166(1 Pt 1):173–180

Basson MA, Echevarria D et al (2008) Specific regions within the embryonic midbrain and cerebellum require different levels of FGF signaling during development. Development 135(5):889–898

Battin M., Rutherford MA, (2001). MRI of the Fetal Brain. MA, Rutherford, Saunders Ltd.: 36–45

Battin MR, Maalouf EF et al (1998) Magnetic resonance imaging of the brain in very preterm infants: visualization of the germinal matrix, early myelination, and cortical folding. Pediatrics 101(6):957–962

Ben-Ari Y, Khalilov I et al (2004) Interneurons set the tune of developing networks. Trends Neurosci 27(7):422–427

Berman JI, Mukherjee P et al (2005) Quantitative diffusion tensor MRI fiber tractography of sensorimotor white matter development in premature infants. Neuroimage 27(4):862–871

Brazel CY, Romanko MJ et al (2003) Roles of the mammalian subventricular zone in brain development. Prog Neurobiol 69(1):49–69

Brisse H, Fallet C et al (1997) Supratentorial parenchyma in the developing fetal brain: in vitro MR study with histologic comparison. AJNR Am J Neuroradiol 18(8):1491–1497

Bronen RA, Cheung G (1991) MRI of the temporal lobe: normal variations, with special reference toward epilepsy. Magn Reson Imaging 9(4):501–507

Brugger PC, Stuhr F et al (2006) Methods of fetal MR: beyond T2-weighted imaging. Eur J Radiol 57(2):172–181

Bui T, Daire JL et al (2006) Microstructural development of human brain assessed in utero by diffusion tensor imaging. Pediatr Radiol 36(11):1133–1140

Bystron I, Rakic P et al (2006) The first neurons of the human cerebral cortex. Nat Neurosci 9(7):880–886

Bystron I, Blakemore C et al (2008) Development of the human cerebral cortex: Boulder Committee revisited. Nat Rev Neurosci 9(2):110–122

Cardoza GR, Goldstein RB, Filly RA (1988) Exclusion of fetal ventriculomegaly with a single measurement: the width of the lateral ventricular atrium. Radiology 169(3):711–714

Chi JG, Dooling EC et al (1977) Gyral development of the human brain. Ann Neurol 1(1):86–93

Childs AM, Ramenghi LA et al (2001) Cerebral maturation in premature infants: quantitative assessment using MR imaging. AJNR Am J Neuroradiol 22(8):1577–1582

Chong BW, Babcook CJ et al (1996) A magnetic resonance template for normal neuronal migration in the fetus. Neurosurgery 39(1):110–116

Chong BW, Babcook CJ et al (1997) A magnetic resonance template for normal cerebellar development in the human fetus. Neurosurgery 41(4):924–928, discussion 928-9

Chung R, Kasprian G et al (2009) The current state and future of fetal imaging. Clin Perinatol 36(3):685–699

Coleman KA, Mitrofanis J (1999) Does the perireticular thalamic nucleus project to the neocortex? Anat Embryol (Berl) 200(5):521–531

Corbin JG, Nery S et al (2001) Telencephalic cells take a tangent: non-radial migration in the mammalian forebrain. Nat Neurosci 4(Suppl):1177–1182

Counsell SJ, Maalouf EF et al (2002) MR imaging assessment of myelination in the very preterm brain. AJNR Am J Neuroradiol 23(5):872–881

Daffos F, Forestier F et al (1988) Fetal curarization for prenatal magnetic resonance imaging. Prenat Diagn 8(4):312–314

Del Rio JA, Martinez A et al (2000) Developmental history of the subplate and developing white matter in the murine neocortex. Neuronal organization and relationship with the main afferent systems at embryonic and perinatal stages. Cereb Cortex 10(8):784–801

Dorovini-Zis K, Dolman CL (1977) Gestational development of brain. Arch Pathol Lab Med 101(4):192–195

Dubois J, Benders M et al (2008) Mapping the early cortical folding process in the preterm newborn brain. Cereb Cortex 18(6):1444–1454

Earle KL, Mitrofanis J (1996) Genesis and fate of the perireticular thalamic nucleus during early development. J Comp Neurol 367(2):246–263

Eyre JA, Miller S et al (2000) Functional corticospinal projections are established prenatally in the human foetus permitting involvement in the development of spinal motor centres. Brain 123(Pt 1):51–64

Farrell TA, Hertzberg BS et al (1994) Fetal lateral ventricles: reassessment of normal values for atrial diameter at US. Radiology 193(2):409–411

Fields RD (2004) Volume transmission in activity-dependent regulation of myelinating glia. Neurochem Int 45(4):503–509

Filly RA, Goldstein RB (1994) The fetal ventricular atrium: fourth down and 10 mm to go. Radiology 193(2): 315–317

Fischl B, Rajendran N et al (2008) Cortical folding patterns and predicting cytoarchitecture. Cereb Cortex 18(8): 1973–1980

Fishell G, Mason CA et al (1993) Dispersion of neural progenitors within the germinal zones of the forebrain. Nature 362(6421):636–638

Fogliarini C, Chaumoitre K et al (2005) Assessment of cortical maturation with prenatal MRI. Part I: Normal cortical maturation. Eur Radiol 15(8):1671–1685

Garel C (2004) MRI of the fetal brain: normal development and cerebral pathologies. Springer-Verlag, Berlin Heidelberg

Garel C, Alberti C (2006) Coronal measurement of the fetal lateral ventricles: comparison between ultrasonography and magnetic resonance imaging. Ultrasound Obstet Gynecol 27(1):23–27

Garel C, Chantrel E et al (2001) Fetal cerebral cortex: normal gestational landmarks identified using prenatal MR imaging. AJNR Am J Neuroradiol 22(1):184–189

Garel C, Chantrel E et al (2003) Fetal MRI: normal gestational landmarks for cerebral biometry, gyration and myelination. Childs Nerv Syst 19(7–8):422–425

Garel C, Delezoide AL et al (2004) Contribution of fetal MR imaging in the evaluation of cerebral ischemic lesions. AJNR Am J Neuroradiol 25(9):1563–1568

Girard NJ, Raybaud CA (1992) In vivo MRI of fetal brain cellular migration. J Comput Assist Tomogr 16(2):265–267

Girard N, Raybaud C et al (1991) MRI study of brain myelination. J Neuroradiol 18(4):291–307

Girard N, Raybaud C et al (1995) In vivo MR study of brain maturation in normal fetuses. AJNR Am J Neuroradiol 16(2):407–413

Glenn OA, Barkovich AJ (2006) Magnetic resonance imaging of the fetal brain and spine: an increasingly important tool in prenatal diagnosis, part 1. AJNR Am J Neuroradiol 27(8):1604–1611

Grever WE, Chiu FC et al (1996) Quantification of myelin basic protein in the human fetal spinal cord during the midtrimester of gestation. J Comp Neurol 376(2):306–314

Gupta RK, Hasan KM et al (2005) Diffusion tensor imaging of the developing human cerebrum. J Neurosci Res 81(2):172–178

Hankin MH, Silver J (1988) Development of intersecting CNS fiber tracts: the corpus callosum and its perforating fiber pathway. J Comp Neurol 272(2):177–190

Hilgetag CC, Barbas H (2005) Developmental mechanics of the primate cerebral cortex. Anat Embryol (Berl) 210(5–6):411–417

Hofer S, Frahm J (2006) Topography of the human corpus callosum revisited–comprehensive fiber tractography using diffusion tensor magnetic resonance imaging. Neuroimage 32(3):989–994

Huang H, Zhang J et al (2006) White and gray matter development in human fetal, newborn and pediatric brains. Neuroimage 33(1):27–38

Huang H, Xue R et al (2009) Anatomical characterization of human fetal brain development with diffusion tensor magnetic resonance imaging. J Neurosci 29(13):4263–4273

Huppi PS, Maier SE et al (1998) Microstructural development of human newborn cerebral white matter assessed in vivo by diffusion tensor magnetic resonance imaging. Pediatr Res 44(4):584–590

Hynes RO, Patel R et al (1986) Migration of neuroblasts along preexisting axonal tracts during prenatal cerebellar development. J Neurosci 6(3):867–876

Isumi H, Mizuguchi M et al (1997) Differential development of the human cerebellar vermis: immunohistochemical and morphometrical evaluation. Brain Dev 19(4): 254–257

Jakovcevski I, Zecevic N (2005) Olig transcription factors are expressed in oligodendrocyte and neuronal cells in human fetal CNS. J Neurosci 25(44):10064–10073

Joseph R (2000) Fetal brain behavior and cognitive development. Dev Rev 20:81–98

Jovanov-Milosevic N, Culjat M et al (2009) Growth of the human corpus callosum: modular and laminar morphogenetic zones. Front Neuroanat 3:6

Judas M, Rados M et al (2005) Structural, immunocytochemical, and mr imaging properties of periventricular crossroads of growing cortical pathways in preterm infants. AJNR Am J Neuroradiol 26(10):2671–2684

Kasprian G (2006) Growth and development of the fetal temporal lobe in vivo. Medical University of Vienna, Vienna

Kasprian G, Brugger PC et al (2008) In utero tractography of fetal white matter development. Neuroimage 43(2): 213–224

Kasprian G, Langs G et al (2010) The prenatal origin of hemispheric asymmetry: an in utero neuroimaging study. Cereb Cortex. [Epub ahead of print]

Katz MJ, Lasek RJ et al (1983) Ontophyletics of the nervous system: development of the corpus callosum and evolution of axon tracts. Proc Natl Acad Sci USA 80(19): 5936–5940

Khazipov R, Esclapez M et al (2001) Early development of neuronal activity in the primate hippocampus in utero. J Neurosci 21(24):9770–9781

Kier EL, Truwit CL (1996) The normal and abnormal genu of the corpus callosum: an evolutionary, embryologic, anatomic, and MR analysis. AJNR Am J Neuroradiol 17(9): 1631–1641

Kier EL, Truwit CL (1997) The lamina rostralis: modification of concepts concerning the anatomy, embryology, and MR appearance of the rostrum of the corpus callosum. AJNR Am J Neuroradiol 18(4):715–722

Kier EL, Kim JH et al (1997) Embryology of the human fetal hippocampus: MR imaging, anatomy, and histology. AJNR Am J Neuroradiol 18(3):525–532

Kinney HC (2005) Human myelination and perinatal white matter disorders. J Neurol Sci 228(2):190–192

Kinoshita Y, Okudera T et al (2001) Volumetric analysis of the germinal matrix and lateral ventricles performed using MR images of postmortem fetuses. AJNR Am J Neuroradiol 22(2):382–388

Koester SE, O'Leary DD (1994) Axons of early generated neurons in cingulate cortex pioneer the corpus callosum. J Neurosci 14(11 Pt 1):6608–6620

Kostovic I (1990) Structural and histochemical reorganization of the human prefrontal cortex during perinatal and postnatal life. Prog Brain Res 85:223–239, discussion 239–240

Kostovic I, Jovanov-Milosevic N (2008) Subplate zone of the human brain: historical perspective and new concepts. Coll Antropol 32(Suppl 1):3–8

Kostovic I, Judas M (1998) Transient patterns of organization of the human fetal brain. Croat Med J 39(2):107–114
Kostovic I, Judas M (2002) Correlation between the sequential ingrowth of afferents and transient patterns of cortical lamination in preterm infants. Anat Rec 267(1):1–6
Kostovic I, Judas M (2006) Prolonged coexistence of transient and permanent circuitry elements in the developing cerebral cortex of fetuses and preterm infants. Dev Med Child Neurol 48(5):388–393
Kostovic I, Vasung L (2009) Insights from in vitro fetal magnetic resonance imaging of cerebral development. Semin Perinatol 33(4):220–233
Kostovic I, Judas M et al (1995) Ontogenesis of goal-directed behavior: anatomo-functional considerations. Int J Psychophysiol 19(2):85–102
Kostovic I, Judas M et al (2002) Laminar organization of the human fetal cerebrum revealed by histochemical markers and magnetic resonance imaging. Cereb Cortex 12(5): 536–544
Lan LM, Yamashita Y et al (2000) Normal fetal brain development: MR imaging with a half-Fourier rapid acquisition with relaxation enhancement sequence. Radiology 215(1):205–210
Larroche JC (1981) Morphological criteria of central nervous system development in the human foetus. J Neuroradiol 8(2):93–108
Le Bihan D, Breton E, Lallemand D, Grenier P, Cabanis E, Laval-Jeantet M (1986) MR imaging of intravoxel incoherent motions: application to diffusion and perfusion in neurologic disorders. Radiology 161(2):401–407
Lent R, Uziel D et al (2005) Cellular and molecular tunnels surrounding the forebrain commissures of human fetuses. J Comp Neurol 483(4):375–382
Letinic K, Kostovic I (1997) Transient fetal structure, the gangliothalamic body, connects telencephalic germinal zone with all thalamic regions in the developing human brain. J Comp Neurol 384(3):373–395
Letinic K, Rakic P (2001) Telencephalic origin of human thalamic GABAergic neurons. Nat Neurosci 4(9):931–936
Letinic K, Zoncu R et al (2002) Origin of GABAergic neurons in the human neocortex. Nature 417(6889):645–649
Levine D, Barnes PD (1999) Cortical maturation in normal and abnormal fetuses as assessed with prenatal MR imaging. Radiology 210(3):751–758
Levine D, Trop I et al (2002) MR imaging appearance of fetal cerebral ventricular morphology. Radiology 223(3): 652–660
Levitt P (2003) Structural and functional maturation of the developing primate brain. J Pediatr 143(4 Suppl):S35–S45
Lindwall C, Fothergill T et al (2007) Commissure formation in the mammalian forebrain. Curr Opin Neurobiol 17(1):3–14
Lowery CL, Hardman MP et al (2007) Neurodevelopmental changes of fetal pain. Semin Perinatol 31(5):275–282
Maas LC, Mukherjee P et al (2004) Early laminar organization of the human cerebrum demonstrated with diffusion tensor imaging in extremely premature infants. Neuroimage 22(3): 1134–1140
Manganaro L, Perrone A et al (2007) Evaluation of normal brain development by prenatal MR imaging. Radiol Med 112(3):444–455
Marin O, Rubenstein JL (2003) Cell migration in the forebrain. Annu Rev Neurosci 26:441–483
Marin-Padilla M (1990) Three-dimensional structural organization of layer I of the human cerebral cortex: a Golgi study. J Comp Neurol 299(1):89–105
Marin-Padilla M (1998) Cajal-Retzius cells and the development of the neocortex. Trends Neurosci 21(2):64–71
McKinstry RC, Mathur A et al (2002) Radial organization of developing preterm human cerebral cortex revealed by noninvasive water diffusion anisotropy MRI. Cereb Cortex 12(12):1237–1243
Menezes JR, Marins M et al (2002) Cell migration in the postnatal subventricular zone. Braz J Med Biol Res 35(12): 1411–1421
Mihajlovic P, Zecevic N (1986) Development of the human dentate nucleus. Hum Neurobiol 5(3):189–197
Molnar Z, Blakemore C (1995) How do thalamic axons find their way to the cortex? Trends Neurosci 18(9):389–397
Mukherjee P, Miller JH et al (2002) Diffusion-tensor MR imaging of gray and white matter development during normal human brain maturation. AJNR Am J Neuroradiol 23(9): 1445–1456
Muller F, O'Rahilly R (1988) The first appearance of the future cerebral hemispheres in the human embryo at stage 14. Anat Embryol (Berl) 177(6):495–511
Nakayama T, Yamada R (1999) MR imaging of the posterior fossa structures of human embryos and fetuses. Radiat Med 17(2):105–114
Nara T, Goto N et al (1996) Morphometric development of the human fetal auditory system: inferior collicular nucleus. Brain Dev 18(1):35–39
Olesen AG, Svare JA (2004) Decreased fetal movements: background, assessment, and clinical management. Acta Obstet Gynecol Scand 83(9):818–826
O'Rahilly R, Muller F (1999) Minireview: summary of the initial development of the human nervous system. Teratology 60(1):39–41
Parazzini C, Righini A et al (2008) Prenatal magnetic resonance imaging: brain normal linear biometric values below 24 gestational weeks. Neuroradiology 50(10):877–883
Partridge SC, Mukherjee P et al (2004) Diffusion tensor imaging: serial quantitation of white matter tract maturity in premature newborns. Neuroimage 22(3):1302–1314
Partridge SC, Mukherjee P et al (2005) Tractography-based quantitation of diffusion tensor imaging parameters in white matter tracts of preterm newborns. J Magn Reson Imaging 22(4):467–474
Penrice J, Cady EB et al (1996) Proton magnetic resonance spectroscopy of the brain in normal preterm and term infants, and early changes after perinatal hypoxia-ischemia. Pediatr Res 40(1):6–14
Petanjek Z, Dujmovic A et al (2008) Distinct origin of GABAergic neurons in forebrain of man, nonhuman primates and lower mammals. Coll Antropol 32(Suppl 1):9–17
Plachez C, Richards LJ (2005) Mechanisms of axon guidance in the developing nervous system. Curr Top Dev Biol 69: 267–346
Prayer D, Prayer L (2003) Diffusion-weighted magnetic resonance imaging of cerebral white matter development. Eur J Radiol 45(3):235–243
Prayer D, Brugger PC et al (2005) Triangular crossroads: a "Wetterwinkel" of the fetal brain. American Society of Neuroradiology, Toronto

Prayer D, Kasprian G et al (2006) MRI of normal fetal brain development. Eur J Radiol 57(2):199–216
Rados M, Judas M et al (2006) In vitro MRI of brain development. Eur J Radiol 57(2):187–198
Rakic P (2003) Developmental and evolutionary adaptations of cortical radial glia. Cereb Cortex 13(6):541–549
Rakic P (2004) Neuroscience. Genetic control of cortical convolutions. Science 303(5666):1983–1984
Rakic P, Yakovlev PI (1968) Development of the corpus callosum and cavum septi in man. J Comp Neurol 132(1):45–72
Raybaud C (2010) The corpus callosum, the other great forebrain commissures, and the septum pellucidum: anatomy, development, and malformation. Neuroradiology 52(6):447–477
Ren T, Anderson A et al (2006) Imaging, anatomical, and molecular analysis of callosal formation in the developing human fetal brain. Anat Rec A Discov Mol Cell Evol Biol 288(2):191–204
Richards LJ (2002) Axonal pathfinding mechanisms at the cortical midline and in the development of the corpus callosum. Braz J Med Biol Res 35(12):1431–1439
Richards LJ, Koester SE et al (1997) Directed growth of early cortical axons is influenced by a chemoattractant released from an intermediate target. J Neurosci 17(7): 2445–2458
Richards LJ, Plachez C et al (2004) Mechanisms regulating the development of the corpus callosum and its agenesis in mouse and human. Clin Genet 66(4):276–289
Righini A, Bianchini E et al (2003) Apparent diffusion coefficient determination in normal fetal brain: a prenatal MR imaging study. AJNR Am J Neuroradiol 24(5):799–804
Righini A, Zirpoli S et al (2006) Hippocampal infolding angle changes during brain development assessed by prenatal MR imaging. AJNR Am J Neuroradiol 27(10): 2093–2097
Righini A, Parazzini C et al (2009) Prenatal MR imaging of the normal pituitary stalk. AJNR Am J Neuroradiol 30(5): 1014–1016
Rutherford M, Jiang S et al (2008) MR imaging methods for assessing fetal brain development. Dev Neurobiol 68(6): 700–711
Samuelsen GB, Larsen KB et al (2003) The changing number of cells in the human fetal forebrain and its subdivisions: a stereological analysis. Cereb Cortex 13(2):115–122
Sasaki M, Sone M et al (1993) Hippocampal sulcus remnant: potential cause of change in signal intensity in the hippocampus. Radiology 188(3):743–746
Schmook MT, Brugger PC et al (2010) Forebrain development in fetal MRI: evaluation of anatomical landmarks before gestational week 27. Neuroradiology 52(6):495–504
Schneider JF, Confort-Gouny S et al (2007) Diffusion-weighted imaging in normal fetal brain maturation. Eur Radiol 17(9):2422–2429
Schneider MM, Berman JI et al (2009) Normative apparent diffusion coefficient values in the developing fetal brain. AJNR Am J Neuroradiol 30(9):1799–1803
Shen WB, Plachez C et al (2006) Identification of candidate genes at the corticoseptal boundary during development. Gene Expr Patterns 6(5):471–481
Shiraishi K, Itoh M et al (2003) Myelination of a fetus with Pelizaeus-Merzbacher disease: immunopathological study. Ann Neurol 54(2):259–262
Shu T, Richards LJ (2001) Cortical axon guidance by the glial wedge during the development of the corpus callosum. J Neurosci 21(8):2749–2758
Shu T, Puche AC et al (2003) Development of midline glial populations at the corticoseptal boundary. J Neurobiol 57(1):81–94
Sidman RL, Rakic P (1973) Neuronal migration, with special reference to developing human brain: a review. Brain Res 62(1):1–35
Silver J, Lorenz SE et al (1982) Axonal guidance during development of the great cerebral commissures: descriptive and experimental studies, in vivo, on the role of preformed glial pathways. J Comp Neurol 210(1):10–29
Simonati A, Tosati C et al (1999) Cell proliferation and death: morphological evidence during corticogenesis in the developing human brain. Microsc Res Tech 45(6):341–352
Sotelo C (2004) Cellular and genetic regulation of the development of the cerebellar system. Prog Neurobiol 72(5):295–339
Sparling JW, Van Tol J et al (1999) Fetal and neonatal hand movement. Phys Ther 79(1):24–39
Stazzone MM, Hubbard AM et al (2000) Ultrafast MR imaging of the normal posterior fossa in fetuses. AJR Am J Roentgenol 175(3):835–839
Super H, Uylings HB (2001) The early differentiation of the neocortex: a hypothesis on neocortical evolution. Cereb Cortex 11(12):1101–1109
Sur M, Rubenstein JL (2005) Patterning and plasticity of the cerebral cortex. Science 310(5749):805–810
ten Donkelaar HJ (2000) Major events in the development of the forebrain. Eur J Morphol 38(5):301–308
ten Donkelaar HJ, Lammens M (2009) Development of the human cerebellum and its disorders. Clin Perinatol 36(3): 513–530
ten Donkelaar HJ, Lammens M et al (2003) Development and developmental disorders of the human cerebellum. J Neurol 250(9):1025–1036
Tilea B, Alberti C et al (2009) Cerebral biometry in fetal magnetic resonance imaging: new reference data. Ultrasound Obstet Gynecol 33(2):173–181
Toi A, Lister WS et al (2004) How early are fetal cerebral sulci visible at prenatal ultrasound and what is the normal pattern of early fetal sulcal development? Ultrasound Obstet Gynecol 24(7):706–715
Toro R, Burnod Y (2005) A morphogenetic model for the development of cortical convolutions. Cereb Cortex 15(12):1900–1913
Triulzi F, Parazzini C et al (2005) MRI of fetal and neonatal cerebellar development. Semin Fetal Neonatal Med 10(5):411–420
Tulay CM, Elevli L et al (2004) Morphological study of the perireticular nucleus in human fetal brains. J Anat 205(1): 57–63
Twickler DM, Reichel T et al (2002) Fetal central nervous system ventricle and cisterna magna measurements by magnetic resonance imaging. Am J Obstet Gynecol 187(4):927–931
Ulfig N (2000) The ganglionic eminence – new vistas. Trends Neurosci 23(11):530
Ulfig N (2002) The ganglionic eminence – a putative intermediate target of amygdaloid connections. Brain Res Dev Brain Res 139(2):313–318
van der Knaap MS, van Wezel-Meijler G et al (1996) Normal gyration and sulcation in preterm and term neonates: appearance on MR images. Radiology 200(2):389–396

Van Essen DC (1997) A tension-based theory of morphogenesis and compact wiring in the central nervous system. Nature 385(6614):313–318

Widjaja E, Geibprasert S et al (2010a) Alteration of human fetal subplate layer and intermediate zone during normal development on MR and diffusion tensor imaging. AJNR Am J Neuroradiol 31(6):1091–1099

Widjaja E, Geibprasert S et al (2010b) Corroboration of normal and abnormal fetal cerebral lamination on postmortem MR imaging with postmortem examination. AJNR Am J Neuroradiol 0: ajnr.A2193v1-0

Wimberger DM, Roberts TP et al (1995) Identification of "premyelination" by diffusion-weighted MRI. J Comput Assist Tomogr 19(1):28–33

Yamaguchi K, Goto N (1997) Three-dimensional structure of the human cerebellar dentate nucleus: a computerized reconstruction study. Anat Embryol (Berl) 196(4):343–348

Yoo SS, Park HJ et al (2005) In vivo visualization of white matter fiber tracts of preterm- and term-infant brains with diffusion tensor magnetic resonance imaging. Invest Radiol 40(2):110–115

Zecevic N (1993) Cellular composition of the telencephalic wall in human embryos. Early Hum Dev 32(2–3): 131–149

Zecevic N, Milosevic A et al (1999) Early development and composition of the human primordial plexiform layer: An immunohistochemical study. J Comp Neurol 412(2): 241–254

Zhai G, Lin W et al (2003) Comparisons of regional white matter diffusion in healthy neonates and adults performed with a 3.0-T head-only MR imaging unit. Radiology 229(3): 673–681